THE ASTRONOMICAL JOURNAL VOLUME 105, NUMBER 3 MARCH 1993

THE FRAGMENTATION OF SMALL ASTEROIDS IN THE ATMOSPHERE

JACK G. HILLS AND M. PATRICK GODA[1]

Theoretical Astrophysics Group, Mail Stop B288, Theoretical Division, Los Alamos National Laboratory, Los Alamos, New Mexico 87545

Received 26 August 1992

ABSTRACT

The fragmentation of a small asteroid in the atmosphere greatly increases its cross-sections for aerodynamic braking and energy dissipation. The differential pressure across a meteoroid disperses its fragments at a velocity that increases with atmospheric density and impact velocity and decreases with meteoroid density. At a typical impact velocity of 22 km/s, the atmosphere absorbs more than half the kinetic energy of stony meteoroids with diameters, $D_M < 220$ m and iron meteoroids with $D_M < 80$ m. The corresponding diameter for comets with impact velocity 50 km/s is $D_M < 1600$ m. Most of this energy dissipation occurs in a fraction of a scale height, which causes large meteoroids to appear to "explode" or "flare" at the end of their visible paths. The dissipation of energy in the atmosphere protects the Earth from direct impact damage (e.g., craters), but the blast wave produced by the dissipation in the atmosphere can cause considerable damage to structures on the ground. The area of destruction around the impact point in which the over pressure in the blast wave exceeds 4 pounds/inch$^2 = 2.8 \times 10^5$ dynes/cm^3, which is enough to knock over trees and destroy buildings, increases rapidly from zero for chondritic meteoroids less than 56 m in diameter (15 megatons) to about 2000 square km for those 80 m in diameter (48 megatons). (The minimum diameter of the Tunguska impactor of 1908 is about 80 m.) The area of destruction produced by stony asteroids between 70 and 200 m in diameter is up to twice as great as it would be without fragmentation. Crater formation and earthquakes are not significant in land impacts by stony asteroids less than about 200 m in diameter because of the air protection. The situation is similar for the production of water waves and tsunami for ocean impacts. Tsunami is probably the most devastating type of damage for asteroids that are 200 m to 1 km in diameter. An impact by an asteroid this size anywhere in the Atlantic would devastate coastal areas on both sides of ocean. The atmosphere plume produced by asteroids with diameters exceeding about 120 m cannot be contained by the atmosphere, so this bubble of high-entropy gas forms a new layer on top of the atmosphere. The dust entrapped in this hot gas is likely to have optical depths exceeding $\tau = 10$ for asteroids with diameters exceeding about 0.5–1 km. The optical flux from asteroids 60 m or more in diameter is enough to ignite pine forests. However, the blast wave from an impacting asteroid goes beyond the radius in which the fire starts. The blast wave tends to blow out the fire, so it is likely that the impact will char the forest (as at Tunguska), but the impact will not produce a sustained fire. Because comets dissipate their energy much higher in the atmosphere than asteroids, they illuminate a much larger region and their blast wave is weaker, so they are much more effective in producing large fires. This suggests that the Cretaceous–Tertiary impactor was a comet rather than an asteroid.

1. INTRODUCTION

Fragmentation is one of the major problems of meteor research (Bronshten 1983). A quantitative model of fragmentation that accounts for its effect on the dynamics of a meteor is lacking in the literature. This paper addresses this problem.

Large stony meteorites fragment and scatter over an area of up to several square kilometers. The biggest stony meteorites that have been recovered are less massive than 500 kg. Fragmentation causes most of the energy of stony (and iron) meteorites up to many meters across to be dissipated in the atmosphere rather than at ground impact.

This atmospheric protection greatly reduces the economic damage done by the smaller asteroids. Determining the amount of this atmospheric protection for small asteroid impacts is one of the primary motivations for this research. Even for very small meteorites, economic damage is one of the primary means of detecting recent meteorite falls. Of the sixteen known meteorite falls in the United States and Canada between 1965 and 1985, seven falls were detected because of the damage they inflicted on buildings, an additional one hit a house without damaging it, and another damaged a mailbox (Halliday *et al.* 1985). While falls that produced economic damage are only a small fraction of the meteorites that must have fallen during this time interval, half of the recorded falls were detected from the economic damage they produced. We shall estimate the damage caused by small asteroids both to find the damage

[1]Now at Wabash College, Crawfordsville, IN.

 0004-6256/93/031114-31$00.90

expected from future asteroid impacts and to discover signatures of asteroid falls that may allow us to identify past impacts in the geophysical record of the Earth.

In this paper we develop a model of the atmospheric fragmentation of large meteoroids (asteroids) that quantitatively reproduces many of the observed properties of fragmenting large meteoroids. We shall first introduce our fragmentation model and discuss some of its consequences by using analytic approximations. We then discuss the results derived by putting the fragmentation model into a computer code that models the dynamics of the meteor in the atmosphere.

2. THE FRAGMENTATION MODEL

A meteoroid passing through the atmosphere begins to fragment when the aerodynamic pressure, P, exceeds its material strength. Cracks in it spread and accrete to form voids that grow until they expose individual fragments of the original body. As these fragments expand apart, the meteoroid first appears in projection as a solid (optically thick) object of increasing size and roughness. Aerodynamically, it acts as one body with a single bow shock in front of it. Its increasing size causes a steady increase in its aerodynamic braking.

The dissociating meteoroid continues to act aerodynamically as a single object until it has expanded to some critical value R_c where voids begin to appear between the fragments as viewed in projection. These voids allow gas to stream between the individual fragments, so the fragments develop their own bow shocks to become independent aerodynamic objects in the atmosphere. The cross-sectional area of the fragmented meteoroid, πR_c^2, at the critical radius is about equal to the projected areas of the individual fragments. Using the distribution of masses found in various classical fragmentation situations (Brown 1988) and adding up the cross-sectional areas of the fragments with radii at least 0.01 that of the largest fragment, we find that $R_c \approx 2R_0$, where R_0 is the radius of the meteoroid before breakup. As we shall show, the actual value of (R_c/R_0) is not important for the larger meteoroids that undergo several successive fragmentations.

The expanding radius of the debris cloud causes a rapid increase in the aerodynamic braking. The effective cross sectional (drag) radius of the meteoroid increases while its mass remains constant. When the radius of the meteoroid debris cloud has expanded to R_c, each fragment is no longer aerodynamically shielded by its fellow fragments, so it feels a differential force across it comparable to the stagnation pressure. If the debris cloud has slowed enough that this ram pressure is less than the fragmentation pressure, each piece will then descend independently without further fragmentation. This is generally true of "smaller" meteoroids (initial radius $R_0 < 1$–2 m).

If, when the radius, r_d, of the debris cloud has grown to R_c, the meteoroid debris cloud has not slowed enough for $P_{\rm ram}$, the ram pressure, to have dropped below the critical fragmentation pressure, S, each fragment undergoes further fragmentation. This is case for the large meteoroids (small asteroids), which are our primary concern in this paper. The fragments break into smaller pieces when the projected expanding cross-section of the original meteor starts to show open voids (when $r_d = R_c \approx 2R_0$). Because the expansion velocity of the debris increases with increasing atmospheric density, the expanding debris will tend to fill in the holes between the fragments, so the cloud of fragments always looks nearly optically thick to the bow shock. This process continues until the swarm, as a whole, has slowed enough that $P_{\rm ram} < S$. Only then do the individual pieces develop their own bow shock and the fragments finally separate from each other. Large asteroids undergo several stages of fragmentation before they reach the ground. In this continuous fragmentation model, the exact value of R_c/R_0 is not important if $R_{\rm frag} \gg R_c$, where $R_{\rm frag}$ is value of r_d when $P_{\rm ram}$ drops below S. For meteor radius $R < R_{\rm frag}$, we treat the breakup as a continuous process in which there is a progressive increase in the radius of the debris cloud, a decrease in the maximum size of the fragments and a progressive increase in the aerodynamic braking. When $r_d = R_{\rm frag}$, no further fragmentation occurs. We assume that the existing fragments become decoupled from the common bow shock when $r_d = 2R_{\rm frag}$.

If $\mathscr{M}$ is the remaining mass of the meteorite debris after ablation, the largest radius of any fragment when the fragmentation stops is about

$$S_{\rm max} \approx \left(\frac{\mathscr{M}}{\frac{4}{3}\pi R_{\rm frag}^2 \rho_{\mathscr{M}}} \right) = R_0 \left(\frac{R_0}{R_{\rm frag}} \right)^2 \left(\frac{\mathscr{M}}{\mathscr{M}_0} \right), \quad (1)$$

where $\mathscr{M}_0$ and R_0 are the mass and radius of the asteroid before it enters the atmosphere. Here we treat the asteroid debris as spheroid of mass $\mathscr{M}$ and density $\rho_{\mathscr{M}}$ with $R_{\rm frag}$ being the equatorial radius of the swarm when fragmentation stops. The fragment of radius $S_{\rm max}$ is the maximum size meteorite that we expect to recover from the meteorite fall (assuming the fragmentation stops far enough above the ground that the individual fragments can slow enough behind their individual bow shocks to survive their impact with the ground). The maximum mass of any fragment is about

$$\mathscr{M}_{\rm max} = \mathscr{M}_0 \left(\frac{S_{\rm max}}{R_0} \right)^3. \quad (2)$$

Large objects undergo several successive fragmentations, which accounts for the relatively low masses of stony meteorites.

2.1 Height of Initial Breakup

Fragmentation begins when the ram pressure, $P_{\rm ram}$, at the stagnation point in front of the meteoroid reaches the material strength S of the meteoroid. At this point

$$S = P_{\rm ram} = \rho_{\rm air} V^2, \quad (3)$$

where V is the current velocity of the meteoroid and $\rho_{\rm air}$ is the local air density. The strengths of typical dustballs (presumably comet debris with the ice removed) is about $S = 1 \times 10^7$ dynes/cm^2, that of stony (chondritic) meteor-

ites is about $S=1\text{–}5\times10^8$ dynes/cm^2, and nickel–iron meteorites have $S=2\times10^9$ dynes/cm^2 (Bronshten 1983). We assume that the S of comets is comparable to that of dustballs since ice by itself has a much lower material strength. The dustball material acts as the rebar holding the comets together.

The large meteoroids that are of primary interest in this paper do not slow down significantly prior to fragmentation. The large energy dissipation in the atmosphere after fragmentation occurs in the lower atmosphere, where the decrease in density, ρ, with height can be approximated by the exponential

$$\rho_{\rm air}=\rho_0 e^{-h/H}, \tag{4}$$

where $\rho_0=0.001293$ g/cm^3 is the atmospheric density at $h=0$ and the scale height $H\approx8$ km. From Eqs. (3) and (4), we find that the critical height at which the ram pressure equals the material strength occurs at

$$h_{\rm break}=\ln\left(\frac{\rho_0 V^2}{S}\right)H=\ln\left(\frac{P_{\rm max}}{S}\right)H, \tag{5}$$

where

$$P_{\rm max}=\rho_0 V^2=5.17\times10^9 \text{ dynes/cm}^2 \ (V/20 \text{ km/s})^2 \tag{6}$$

is the maximum possible ram pressure on the asteroid. (This would be its ram pressure just before it hits the ground if it does not slow down in the atmosphere.) Here V is the velocity of the asteroid at height $h_{\rm break}$.

The smallest possible value of V_0, the value of V at the top of the atmosphere is $V_0=11.2$ km/s, which corresponds to a parabolic encounter with the Earth. For $V=V_0$, this gives $P_{\rm max}=1.62\times10^9$ dynes/cm^2. At this velocity, the initial breakup height is $h_{\rm break}=41$ km for dustballs and comets and 22 to 9.4 km for stony meteorites, but at this velocity, nickel–iron meteoroids can reach sea level without breakup. The heights of initial fragmentation increase with V. For $V=20$ km/s, which is typical of incoming meteorites, $h_{\rm break}=50$ km for dustballs and comets, 32 to 19 km for chondritic material, and 7.6 km for irons. We note that $h_{\rm break}$ is independent of the zenith angle of the meteoroid if it is massive enough that it suffers little velocity loss prior to fragmentation.

Once fragmentation starts, it continues all the way to $h=0$ unless the velocity of the debris cloud slows below the critical value

$$V_{\rm max}=\left(\frac{S}{\rho_0}\right)^{1/2}. \tag{7}$$

This gives $V_{\rm max}=2.8$ to 6.2 km/s for stones and 12.4 km/s for irons. Irons with initial impact velocities in the range $V=11.2$ to 12.4 km/s can never fragment.

2.2 Dispersal Velocity of the Fragments

We can estimate the post-breakup dispersal speed, $V_{\rm disp}$, of the meteoroid fragments by dimensional analysis. Each fragment or subfragment is driven from its fellow fragments by the differential pressure across the meteoroid that goes from the full ram pressure at the stagnation point at the front of the meteoroid to zero at the edges. This differential pressure is maintained across the fragmented meteoroid until it has expanded out to a critical radius R_c, where it no longer appears as a coherent body, but each of its subfragments feels its own differential pressure. The total work that has been done on dispersing the swarm by the time it decouples at radius R_c is given by

$$\begin{aligned}\text{Work}&=\text{Force}\times\text{distance}\\ &\approx(\langle\text{Pressure}\rangle\times\text{Area})\times(\text{expansion distance})\\ &\approx(\alpha\rho_{\rm air}V^2)\int_{R_0}^{R_c}\pi r^2\,dr=\frac{\pi\alpha}{3}(\rho_{\rm air}V^2)(R_c^3-R_0^3)\\ &=\frac{7}{3}\pi\alpha\rho_{\rm air}V^2R_0^3\end{aligned} \tag{8}$$

if $R_c=2R_0$. Here α is a dimensionless scaling factor that is on the order of unity and $\rho_{\rm air}$ is the local air density. If we equate the work done to the kinetic energy of expansion of the debris,

$$\frac{1}{2}\mathcal{M}V_{\rm disp}^2=\frac{1}{2}\left(\frac{4\pi}{3}\rho_{\mathcal{M}}R_0^3\right)V_{\rm disp}^2, \tag{9}$$

we find that

$$V_{\rm disp}\approx\left[\frac{7}{2}\alpha\left(\frac{\rho_{\rm air}}{\rho_{\mathcal{M}}}\right)\right]^{1/2}V. \tag{10}$$

We shall assume that $\alpha=1$, so $(7/2)\alpha\approx3.5$. In principle, we can find α empirically by comparing the theoretical dispersal ellipse of meteorites (to be calculated in Sec. 2.3) to that observed, but $\alpha\approx1$ seems consistent with these data. We note that $V_{\rm disp}$ is independent of the initial radius of the meteoroid. $V_{\rm disp}$ increases with $\rho_{\rm air}$ until V drops significantly. As the pieces undergo successive fragmentation, their increasing values of $V_{\rm disp}$ will cause the holes between the fragments to fill in, so the swarm appears optically thick when observed from the front of the bow shock. (Significant holes should appear between the fragments only after the fragmentation stops or when the rate of decrease in the velocity V is larger than the rate of increase in the atmospheric density $\rho_{\rm air}$. In the latter case, the fragments would develop their own bow shocks, but they would continue to fragment.) Equation (10) should adequately model the dispersal velocity until the fragmentation stops.

At sea level, Eq. (10) gives $V_{\rm disp}=V_{\rm SL}\approx0.039$ V for $\rho_{\mathcal{M}}=3$ g/cm^3, which is a typical density for stony meteorites. At the initial height of fragmentation,

$$\begin{aligned}V_{\rm disp}=V_{\rm break}&=\left(\frac{S}{P_{\rm max}}\right)^{1/2}\quad V_{\rm SL}=\left(\frac{S}{\rho_0V^2}\right)^{1/2}V_s\\ &=\left[\frac{7}{2}\alpha\left(\frac{S}{\rho_M}\right)\right]^{1/2}V.\end{aligned} \tag{11}$$

For a stony meteorite with $S=1\times10^8$ dynes/cm^3, this gives $V_{\rm break}=0.14$ $V_{\rm SL}=0.0054$ $V=0.11$ km/s for $V=20$ km/s.

On Venus, where $(\rho_0/\rho_{\mathscr{M}})\approx 0.03$, $V_{\rm disp}\approx 0.32$ V at the bottom of the atmosphere, so the meteoritic fragments scatter over a very large area.

2.3. Radius of the Debris Cloud

After the meteoroid fragments, the radius of its debris cloud as a function of time is given by

$$r_d = R_0 + \int_0^t V_{\rm disp}\, dt, \tag{12}$$

where R_0 is the initial radius of the meteoroid and $V_{\rm disp}$ is its expansion velocity at time t.

In our numerical simulations of the motion of an asteroid through the atmosphere, we have integrated Eq. (12) numerically. We can gain some insight into the meteorite fragmentation problem by determining r_d analytically as a function of height h above the ground in the limit where the meteoroid falls to Earth at zenith angle $\theta=0$. The velocity of the meteoroid through the atmosphere can trivially be related to the rate of change with height by

$$V=-\frac{dh}{dt}, \tag{13}$$

so

$$r_d = R_0 + \int_{h_{\rm break}}^{h_f} -\left(\frac{V_{\rm disp}}{V}\right) dh$$

$$= R_0 + \int_{h_{\rm break}}^{h_f} -\left[\frac{7}{2}\alpha\left(\frac{\rho_{\rm air}}{\rho_{\mathscr{M}}}\right)\right]^{1/2} dh. \tag{14}$$

Here we have used Eq. (10) to find $V_{\rm disp}$. We note that r_d does not depend on V as long as the fragmentation continues. This equation is valid as long as the lower height h_f is greater than the height at which the individual fragments develop their own bow shocks. This occurs where $r_d \geqslant 2R_{\rm frag}$. Here $h_{\rm break}$ is the height at which the meteoroid starts to break up as given by Eq. (5). Using Eq. (4) to evaluate $\rho_{\rm air}$ in Eq. (14) and completing the integral gives

$$r_d = R_0 + R_{\rm max}(e^{-h_f/2H} - e^{-h_{\rm break}/2H}), \tag{15}$$

where

$$R_{\rm max} \equiv 2\left(\frac{7}{2}\alpha\right)^{1/2}\left(\frac{\rho_0}{\rho_{\mathscr{M}}}\right)^{1/2} H. \tag{16}$$

If $h_{\rm break} \gg H$ and the fragmentation continues until impact at sea level, as it does for large impactors, the terminal radius of the debris circle is

$$r_d \rightarrow R_0 + R_{\rm max}. \tag{17}$$

If $\alpha=1$, $h_f=0$, $H=8$ km, and $\rho_0=0.001293$ gm/cm^3, then $R_{\rm max}=0.62$ km for $\rho_{\mathscr{M}}=3$ g/cm^3 and $R_{\rm max}=0.38$ km for $\rho_{\mathscr{M}}=8$ g/cm^3. We note that $R_{\rm max}$ is independent of the impact velocity of the meteoroid because the dispersal velocity is proportional to V while the time the meteoroid spends in going through the atmosphere is inversely proportional to V. We see that stony meteorites with radii less than 0.6 km undergo considerable dispersal in the atmosphere.

If the object stops fragmenting at some finite height, h, then $(r_d - R_0)$ will be smaller than $R_{\rm max}$ because the dispersal velocity given by Eq. (10) applies only until the fragmentation stops. After it stops, the fragments will coast apart at their terminal dispersal velocity. This velocity as well as that of the center of mass will then be reduced by atmospheric friction.

2.3.1 Finite zenith angle

If the meteoroid enters the atmosphere at angle θ from the zenith, the debris pattern becomes an ellipse rather than a circle. The semiminor axis of this ellipse is about $\sec\theta$ times larger than the r_d of an identical meteor entering at $\theta=0$ because the path length through the atmosphere is increased by this factor, which allows it more time to disperse. For a finite zenith angle, we expect the semiminor axis of the debris on impact to be given by

$$R_{\rm minor} = R_0 + R_{\rm max}(e^{-h_f/2H} - e^{-h_{\rm break}/2H})\sec\theta. \tag{18}$$

For a large stony meteorite that fragments continuously from $h_{\rm break}$ to sea level, this reaches a limiting value of

$$R_{\rm minor} = R_0 + R_{\rm max}\sec\theta = R_0 + 0.62 \text{ km } \sec\theta \tag{19}$$

for $h_{\rm break} \gg H$.

If the fragments maintain the original zenith angle θ that they had at the top of the atmosphere, the semimajor axis of the debris ellipse is given by

$$R_{\rm major} = R_{\rm minor}\sec\theta = (R_0 + R_{\rm max}\sec\theta)\sec\theta. \tag{20}$$

In the limit of a large stony meteorite that continues fragmenting to sea level with $h_{\rm break} \gg$ this becomes

$$R_{\rm major} = (R_0 + 0.62 \text{ km } \sec\theta)\sec\theta. \tag{21}$$

2.4 Slowing Down of the Meteoroid Debris in the Atmosphere

We will derive analytic equations describing the motion of the asteroid, although these derivations require simplifications that limit their usefulness. They do provide insight into the problem, and they provide limiting case checks of the full numerical problem.

2.4.1 Dynamics prior to fragmentation

The equation of motion of the meteoroid in the atmosphere before its breakup is given by the equation

$$\mathscr{M}\frac{dV}{dt} = -AC(\rho_{\rm air}V^2) - \mathscr{M}g. \tag{22}$$

Here $A=\pi R^2$ where R is the instantaneous radius of the meteoroid in the atmosphere. We assume that the dimensionless drag coefficient $C=0.5$. Here $\mathscr{M}=[(4/3)\pi R^3\rho_{\mathscr{M}}]$ is the meteoroid mass and $\rho_{\rm air}$ is the local air density. The gravitational acceleration is

$$g=\frac{G\mathcal{M}_\oplus}{(R_\oplus+h)^2}, \tag{23}$$

where $\mathcal{M}_\oplus$ and $R_\oplus$ is the mass and radius of the Earth and h is the height above the Earth.

The mass of the meteorite decreases with time due to ablation as given by the equation

$$\frac{d\mathcal{M}}{dt}=-\sigma C\rho_{\rm air}AV^3, \tag{24}$$

where $\mathcal{M}$, C, A, and V have the same meaning as they do in Eq. (22), and $\sigma\approx 1.0\times10^{-12}$ cgs is the ablation parameter (Bronshten 1983).

We use Equation (4) to determine $\rho_{\rm air}$ as a function of h. We also note that

$$\frac{1}{V}\left(\frac{dV}{dt}\right)=-\left(\frac{dV}{dh}\right). \tag{25}$$

If we put these factors into Eq. (22) and integrate, we find for zenith angle $\theta=0$ and ignoring the gravitational acceleration term, g, that

$$\frac{V_f}{V_0}=\exp\left[-\frac{3}{4}C\left(\frac{\rho_0}{\rho_{\mathcal{M}}}\right)\frac{H}{R}\left(e^{-h_f/H}\right)\right]. \tag{26}$$

2.4.2 Dynamics after fragmentation

After the meteoroid starts to fragment, the effective radius, r_d, of its debris is given by Eq. (14). As long as the debris is not slowed enough to prevent further fragmentation, the debris will remain behind one bow show. In this case, we use Eq. (22) with $A=\pi r_d^2$ to determine the rate of slowing down of the debris prior to the individual pieces developing their own bow shocks.

The change in velocity from the initiation of breakup to any time prior to the termination of this phase is then

$$\int_{V_{\rm break}}^{V_f}\frac{dV}{V}=\int_{h_{\rm break}}^{h_f}\frac{AC}{\mathcal{M}}\rho_0 e^{-h/H}\,dh \tag{27}$$

for $g=0$. Here $A=\pi r_d^2$ is the area of the debris cloud at height h where r_d is given by Eq. (15). We have again ignored ablation. The height h_f cannot be smaller than h_{f_2}, the height at which $r_d=2R_{\rm frag}$ or $h=0$, which ever comes first. Completing the integral, we finally find (with the help of Mathematica) that

$$\frac{V_f}{V_{\rm break}}=\exp\left\{-K\left[\frac{1}{2}(f_h^2-f_b^2)+f_c^2(f_h-f_b)-\frac{4}{3}f_c(f_h^{3/2}-f_b^{3/2})\right]\right\}. \tag{28}$$

Here

$$f_h\equiv e^{-h_f/H},. \tag{29}$$

We note that $f_h\to 1$ as $h_f\to 0$. Also,

$$f_c\equiv\left[f_b^{1/2}-\left(\frac{R_0}{R_{\rm max}}\right)\right] \tag{30}$$

and

$$f_b\equiv e^{-h_{\rm break}/H}=\frac{S}{\rho_0V^2}=\frac{S}{P_{\rm max}}. \tag{31}$$

where S is the material strength and ρ_0V^2 is the ram pressure at sea level. Also,

$$f_b=(1.9\times10^{-3},1.9\times10^{-2},\text{ and }0.39)\left(\frac{20\text{ km/s}}{V}\right)^2 \tag{32}$$

for dustballs, chondritic meteoroids (with $S=1\times10^8$ dynes/cm^2), and nickel–iron meteoroids, respectively. The factor in square brackets in Eq. (28) goes from zero at the initial fragmentation height, $h_{\rm break}$, to about 0.5 at sea level if $h_{\rm break}\gg H$. The first term in square brackets dominates the others if $R_{\rm max}\gg R_0$. The dimensionless term K in Eq. (28) is given by

$$K\equiv\frac{C\pi\rho_0HR_{\rm max}^2}{\mathcal{M}}=\frac{3C\rho_0HR_{\rm max}^2}{4\rho_{\mathcal{M}}R_0^3}=\frac{21\alpha C}{2}\left(\frac{\rho_0}{\rho_{\mathcal{M}}}\right)^2\left(\frac{H}{R_0}\right)^3, \tag{33}$$

where we have used Eq. (16) to find $R_{\rm max}$. The dimensionless drag coefficient C is somewhat larger for the flattened debris than for a spherical meteoroid.

We let

$$s\equiv(h_{\rm break}-h_f) \tag{34}$$

be the distance from the fragmentation height $h_{\rm break}$ to h_f. We then find that

$$f_h=f_be^{s/H}. \tag{35}$$

Using Eqs. (34) and (35), we find that Eq. (28) becomes

$$\frac{V_f}{V_{\rm break}}=\exp\left\{-K\left[\frac{1}{2}f_b^2(e^{2s/H}-1)+f_c^2f_b(e^{s/H}-1)-\frac{4}{3}f_cf_b^{3/2}(e^{3s/2H}-1)\right]\right\}. \tag{36}$$

Equation (36) is only valid as long as the debris cloud has not grown beyond a radius $R_d\geqslant 2R_{\rm frag}$. Once this limit is reached each fragment will acquire its down bow shock and move through the atmosphere independently. We would then have to use Eq. (26) to follow the subsequent deceleration of each fragment.

We have put Eq. (36) in a spreadsheet to test the numerical solutions in the limiting case where $\theta=0$ and the ablation of the meteorite is turned off.

3. NUMERICAL SIMULATIONS

3.1 Numerical Procedure

We have simultaneously integrated the equations of motion, Eq. (22), and ablation, Eq. (24), using a fourth-order Runge–Kutta integrator. We assume that A, the geometric cross section of the object in these two equations, is πR^2 before fragmentation and πr_d^2 after fragmentation starts. Here R is the instantaneous radius of the meteoroid allow-

ing for ablation and r_d is the radius of the debris cloud as given by Eq. (12). When $r_d \geqslant R_{\text{frag}}$ fragmentation stops, and when $r_d \geqslant 2R_{\text{frag}}$ the fragments develop their independent bow shocks. In this post-fragmentation stage, we let R be the radius, $R_{\max}$, of the largest fragment as given by Eq. (1). We follow the motion and radius of this object using the equations of motion and ablation. We assume that the other pieces suffer similar decelerations. This underestimates the deceleration of the other pieces, but in all cases the velocity at the end of the fragmentation phase is much less than the initial velocity, so there is little further deceleration.

We assume that the meteoroid enters the atmosphere at a height $h=100$ km above the Earth, where we specify the initial velocity V_0 and zenith angle θ. The integrations were done in the parallel atmosphere approximation. This is adequate except at very large zenith angles; e.g., it is not adequate for the great meteor of 10 August 1972 that grazed the atmosphere of the Earth at a minimum height of 40 km and then returned to space (Bartky *et al.* 1973). We also assume the exponential atmosphere law given by Eq. (4). In future papers, we will refine the computations by using a true curved atmosphere and tabulated values of atmospheric density with height, but for most large meteorites that dissipate their kinetic energy in the lower atmosphere, the approximations used in this paper should be adequate.

3.2 Energy Dissipation in the Atmosphere

3.2.1 Velocity and kinetic energy reduction

Figure 1 shows the decrease in the velocity of an impactor with height in the atmosphere for stony meteoroids, nickel–iron meteoroids, and dustballs (fluff). These calculations are shown for several impact velocities V_0 at the top of the atmosphere. The impactor has a radius of 50 m, which is a little larger than the Tunguska impactor of 1908. The impactor enters the atmosphere at zenith angle $\theta=0$. Here we have assumed material strengths of $S=1\times10^8$ for weak stones (which are likely to be representative of a majority of chondritic meteoroids), 5×10^8 dynes/cm^2 for hard stones, 2×10^9 dynes/cm^2 for irons, and 1×10^7 dynes/cm^3 for dustballs (comet material with volatiles removed). We assume that the impactors undergo fracturing as long as the ram pressure exceeds S. We assume densities of $\rho_M=3$ g/cm^3 for stones, 8 g/cm^3 for irons, and 0.5 g/cm^3 for dustballs.

Dustballs (fluff) dissipate all their kinetic energy in the atmosphere. Those with impact velocities of 40 km/s or larger are totally burned up (ablated) in the atmosphere, which is why the plots in Fig. 1 terminate at a finite height for these speeds. At lower impact velocities, the unablated material reached terminal velocity. However, comet debris is not likely to have such low velocities.

Stones with high impact velocities lose nearly all their kinetic energy in the atmosphere, but the lower impact velocity ones do not. This ironic situation results from the high-impact-velocity stony meteorites breaking up higher in the atmosphere because their ram pressure reaches the breakup threshold at a lower atmospheric density. The higher the velocity for a given material strength S, the higher up in the atmosphere the object begins to break apart and the larger the cross section of its debris cloud at a given height in the lower atmosphere. Iron meteorites lose much less kinetic energy in the atmosphere because they break up up at much lower heights, so they have less time to produce a debris cloud of sufficiently large cross section (for a meteoroid of this size) to produce much atmospheric braking. As with the stones, the irons with the largest velocities lose the largest fraction of their kinetic energy in the atmosphere.

Figure 2 shows the energy deposited in the atmosphere as a function of height [(megatons of TNT)/km] for the impactors shown in Fig. 1. For nickel–iron meteoroids, the energy deposition in the atmosphere reaches a maximum at $h=0$ (except for $V=30$ km/s), but for the others the maximum occurs at a finite height in the atmosphere. We see from the figure that if most of the energy is deposited in the atmosphere, the bulk of the deposition occurs in a fraction of a scale height, which explains why large stony meteoroids including Tunguska appear to "explode" or flare towards the end of their path. We note that for hard and soft stones, the peak energy deposition rate is 25–30 megatons/km.

The rapid decrease in velocity and the correspondingly large increase in the rate of energy deposition in a narrow range of atmospheric height results from the increasing drag area of the debris cloud due to fragmentation and to the exponential increase in atmospheric density. For large meteoroids, the ratio of the ram pressure to material strength increases rapidly as the impactor plunges deeper into the atmosphere, which makes it easier to continue fragmentation. Figure 3 shows this ratio for the impactors shown in Figs. 1 and 2. We see that this ratio reaches a peak near the height of peak energy deposition and then it rapidly decreases.

The peak in the energy deposition curves of Fig. 2 occur near the height, h_{half}, by which half the kinetic energy has been dissipated. Figure 4 shows h_{half} as a function of impactor radius for various impactor velocities and compositions. The straight-line sections on the left side of each plot are produced by meteoroids that never fragment. These small meteoroids are slowed enough in the upper atmosphere that they never feel enough aerodynamic pressure to fragment. Fragmentation produces a marked increase in the atmospheric drag, so h_{half} is higher in the atmosphere than it would be without fragmentation. Soft stones ($S=10^8$ dynes/cm^3), which are the most common variety, are able to impact the ground with more than half of their impact energy if their radii exceed about 100 to 200 m (depending on impact velocity). We see from an extrapolation of the straight-line portion of Fig. 4 that stones with radii of 10 m would hit the ground with more than half their energy if it were not for fragmentation. Figure 4 shows that only comets with radii exceeding 300 to 1000 m are able to penetrate to the ground with more than half their initial kinetic energy. We note that h_{half} increases with

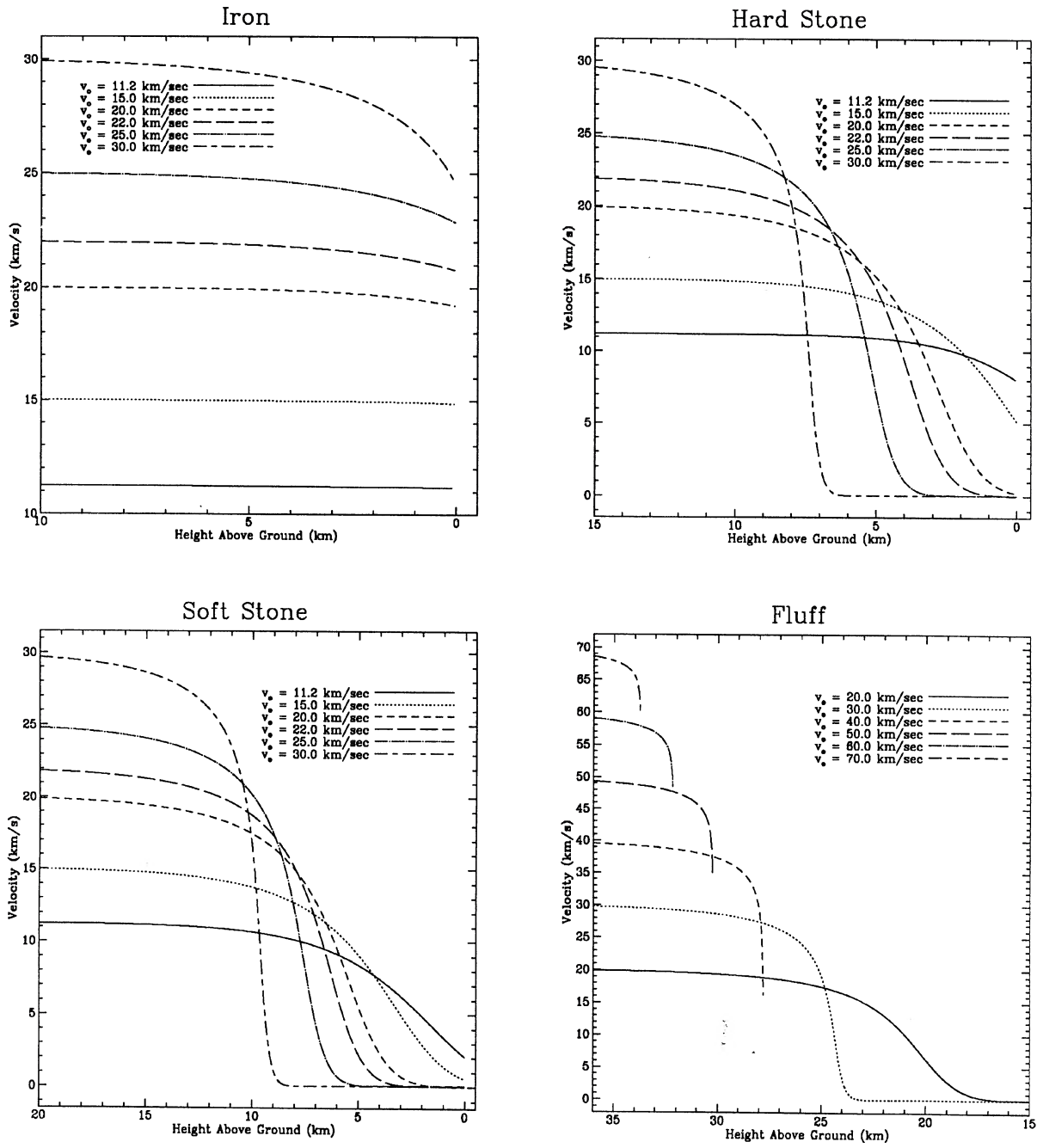

FIG. 1. The decrease in the velocity of an impactor as a function of height in the atmosphere. This is given for a range of initial impact velocities into the upper atmosphere. The stony meteoroids have material strengths of $S=1\times10^8$ dynes/cm^2 (soft) and 5×10^8 dynes/cm^2 (hard) and densities of 3 g/cm^3. The nickel–iron meteoroids have $S=2\times10^9$ dynes/cm^3 and densities of 8 g/cm^3. The dustballs (comets with volatiles removed) have $S=1\times10^7$ dynes/cm^3 and densities of 0.5 g/cm^3. All the impactors have radii $R=50$ m.

impact velocity. This results from the higher velocity impactors breaking up higher in the atmosphere.

Figure 5 shows, as a function of impactor radius, the height of initial fragmentation and the height at which $r_d=2R_{\rm frag}$, where the fragments develop their own independent bow shocks. The value of $h_{\rm half}$ given in Fig. 4 lies between these two heights. Low-mass objects slow down fast enough that they do not fragment at any height. More massive impactors quickly tend to the asymptotic value of $h_{\rm break}$ that corresponds to objects that experience no significant slowing down prior to reaching the aerodynamic pressure needed to start them fragmenting. Low-mass ob-

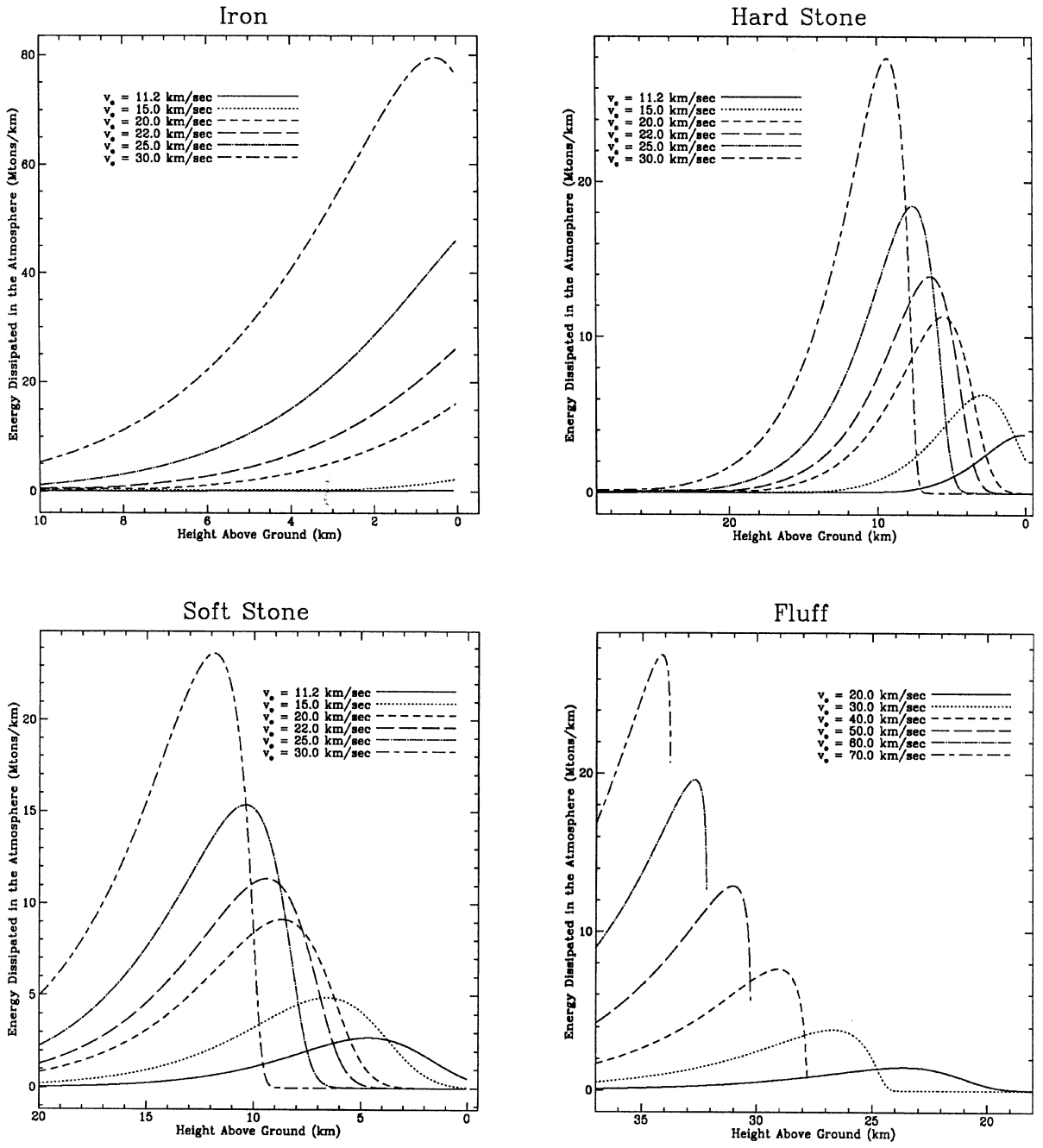

FIG. 2. The energy deposited in the atmosphere as a function of height (megatons/km) by the impactors given in Fig. 1.

jects brake so rapidly after an initial fragmentation that they quickly slow to a velocity that is too low to support further fragmentation. More massive objects continue fragmenting all the way to the ground. Such is the case for large soft-stone asteroids with typical impact velocities of 20 km/s.

While the atmosphere protects the ground from impact damage from moderate size asteroids, the blastwave produced by the energy dissipated in the air can cause considerable damage at ground level. We consider this damage in Sec. *3.5.1.*

3.2.2 Rate of ablation

Figure 6 shows the fraction of the meteoroid mass ablated for the four composition-strength classes given in the earlier figures. The mass fraction ablated is very high and nearly independent of the asteroid radius when the mete-

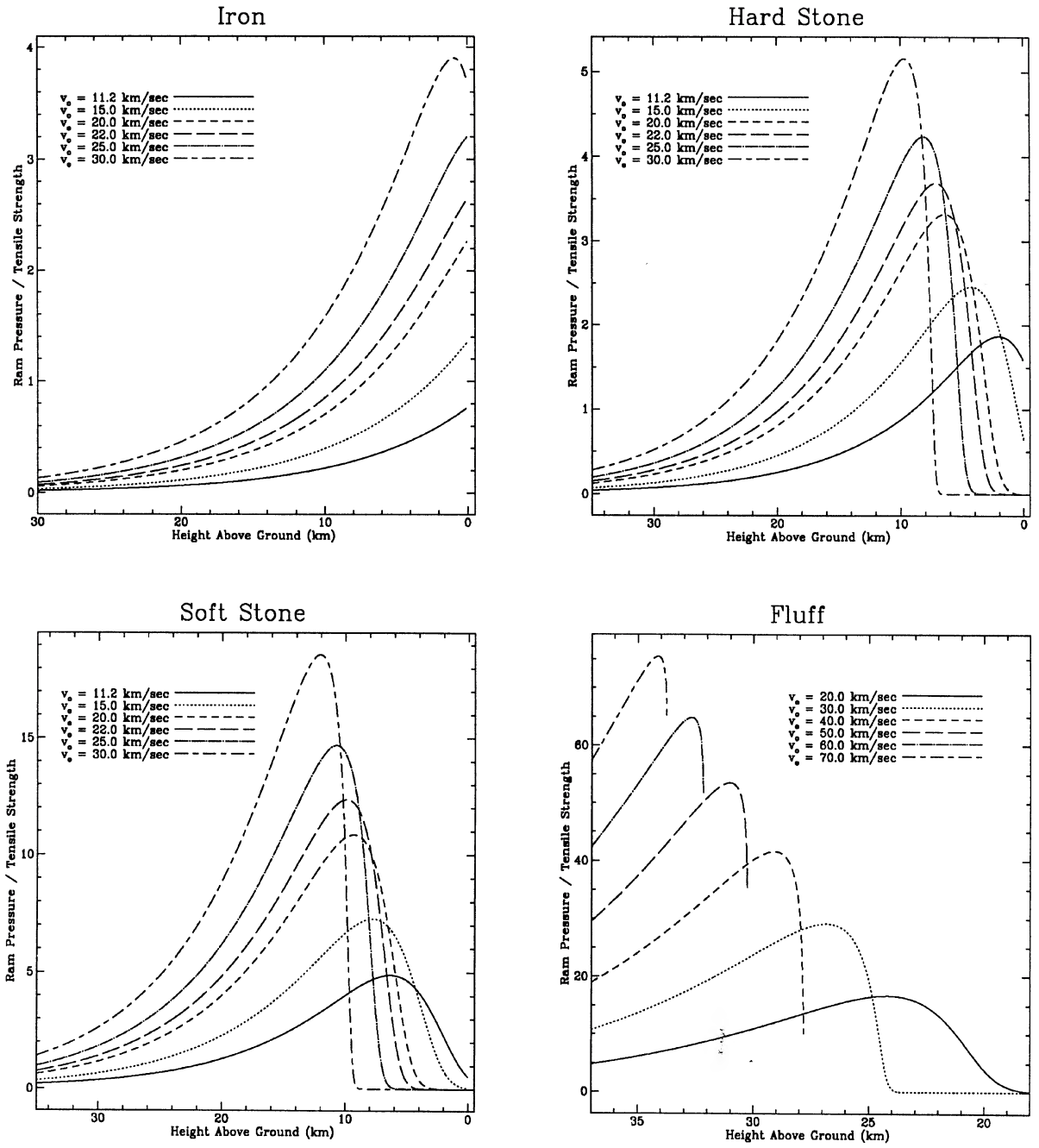

FIG. 3. The ratio of ram pressure to the critical pressure required for fragmentation for the impactors given in Figs. 1 and 2.

oroid loses most of its kinetic energy to the atmosphere. The dips in this plateau, particularly for irons, are due to small impactors that begin to fragment, but slow down so rapidly because of the larger surface area that they decelerate below the velocity needed to sustain fragmentation by the time their initial radius has doubled; e.g., they undergo only one level of fragmentation, rather than continuous fragmentation. For these objects $h_{\rm half}$ nearly coincides with $h_{\rm break}$, so they lose nearly all their kinetic energy at heights just below the initial break point.

Even large nickel–iron meteorites undergo much ablation. The largest known nickel–iron impactor of this century was the Sikhote–Aline meteorite, which fell in Siberia in 1947 (Fessenkov 1955). The meteor produced by this object left behind a very dark wake containing 200 m tons of ablated material. More than 250 fragments with a total weight of over 30 metric tons were recovered on the ground. Fessenkov estimates that the total ground fall may have been up to 100 metric tons if the recovered pieces are corrected for impact erosion, so between 0.65 and 0.85 of

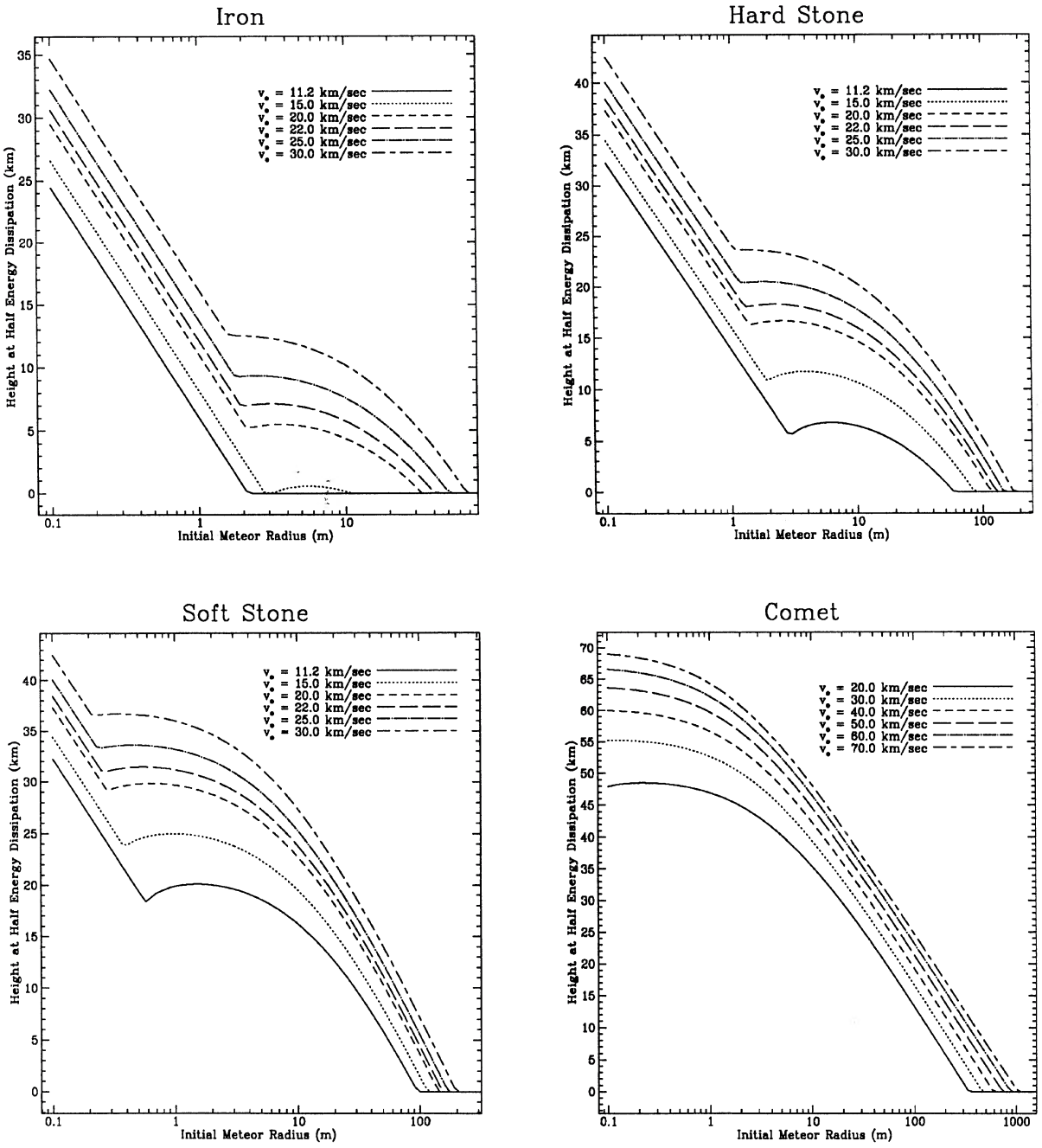

FIG. 4. The height in the atmosphere by which half the impact energy has been dissipated. This is computed as a function of impactor radius for various impact velocities. The composition types are the same as in Fig. 1 except that "comets" have replaced "dustballs" (fluff). Here a comet has the same material strength as a dustball, but its density is 1 g/cm^3.

meteoroid mass was lost by ablation. A 300-ton nickel–iron meteoroid has a radius of about $R=2$ m. We see from Fig. 6 that an iron meteorite of this size produces the observed fraction of ablation if its impact velocity was about $V=18$–22 km/s, which is a reasonable value for a nickel–iron meteorite. A nickel–iron meteoroid with $R=2$ km and $V=11$–15 km/s would ablate only 0.2 to 0.4 of its mass, and it would not fragment if $V<15$ km/s. One coming in at $V\geqslant 30$ km/s would be nearly 100% ablated.

3.2.3. Meteor luminosity

The visual luminosity of the meteor is proportional to its rate of ablation rather than to its rate of energy deposition in the atmosphere (Opik 1958; Bronshten 1983). (We suspect that if the meteor could be observed in the UV from space, its total luminosity would more closely correlate with its power dissipation in the atmosphere.) From Bronshten (1983), the optical luminosity of the meteor is

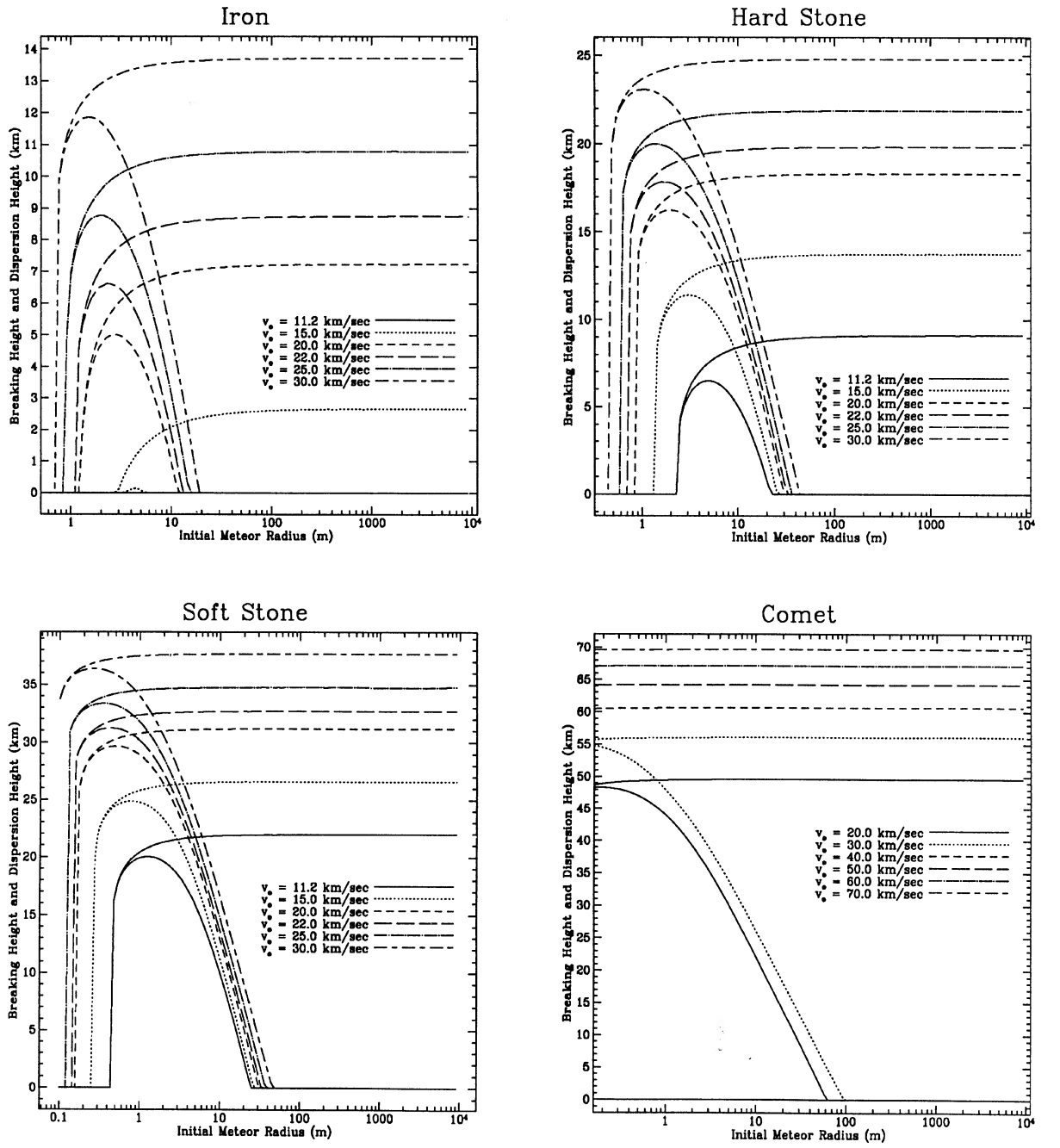

FIG. 5. The height in the atmosphere at which the ram pressure first exceeds the material strength (upper curves) and the height at which $r_d=2R_{\rm frag}$, where the fragments develop their own independent bow shocks. This is computed as a function of impactor radius for various impact velocities using the same composition types as given in Fig. 4.

$$L=\tau\left(-\frac{d\mathcal{M}}{dt}\right)\frac{V^2}{2}, \tag{37}$$

where $d\mathcal{M}/dt$ is the instantaneous rate of ablation. The dimensionless luminosity coefficient, τ, is estimated to range from 3×10^{-4} to 2×10^{-2}. We will assume that $\tau=0.01$.

It is customary to express the visual luminosity in terms of an absolute magnitude, the apparent magnitude as observed at 100 km. Using the calibration in Allen (1973), we find that the visual luminosity is related to the absolute visual magnitude by the equation

$$M_v=-2.5\log_{10}\left[\frac{L}{4\pi(10^7\ \text{cm})^2F_0}\right], \tag{38}$$

where $F_0=3.38\times10^{-6}$ erg s^{-1} cm^{-2} is the visual flux density of a meteor with visual magnitude $m_v=0$.

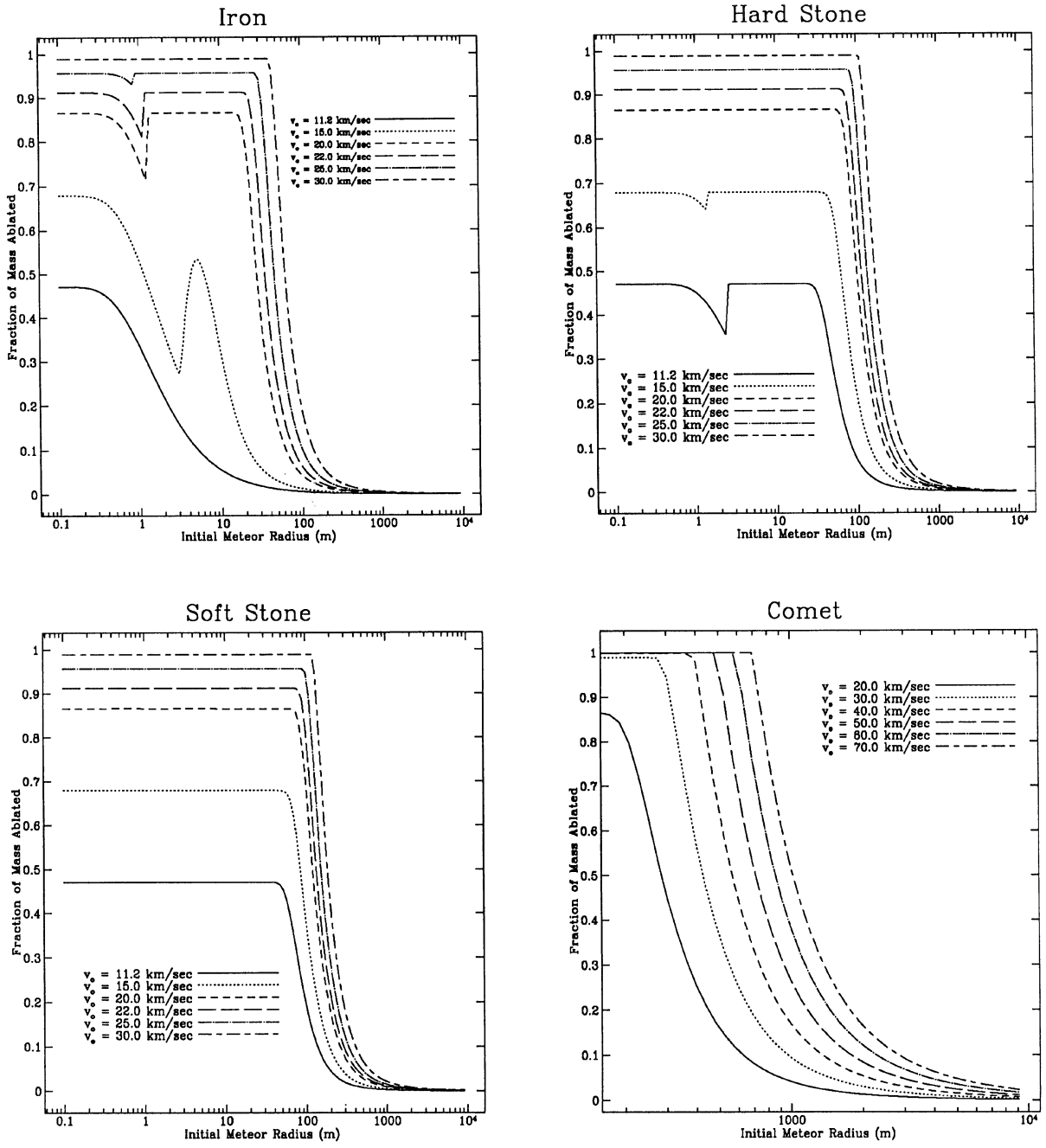

FIG. 6. The fraction of the impactor mass ablated as a function of impactor radius for various impact velocities. This is computed for the composition types shown in the earlier figures.

Figure 7 shows the absolute visual magnitudes of asteroids with radii of 50 m and the composition types given in Figs. 1 and 2. The times are given since the object entered the atmosphere at a height of 100 km. The linear increase in magnitude with time prior to fragmentation is the result of these objects suffering no significant velocity loss, so the increased rate of ablation is due to the exponential increase in the atmospheric density. The lower velocity iron meteorites never leave this stage because they hit the ground without fragmenting. We note the very large increase in magnitude after the object fragments as its surface area and rate of ablation increases. Common (soft) stony meteorites increase more than 5 mag in brightness in less than a second during this flare stage. At common impact velocities of 20–25 km/s, the peak absolute visual magnitudes of these stony meteorites are in the range of -33.5 to -32.5, or 100 times the apparent brightness of the Sun. These magnitudes are a little brighter than the peak brightness of the

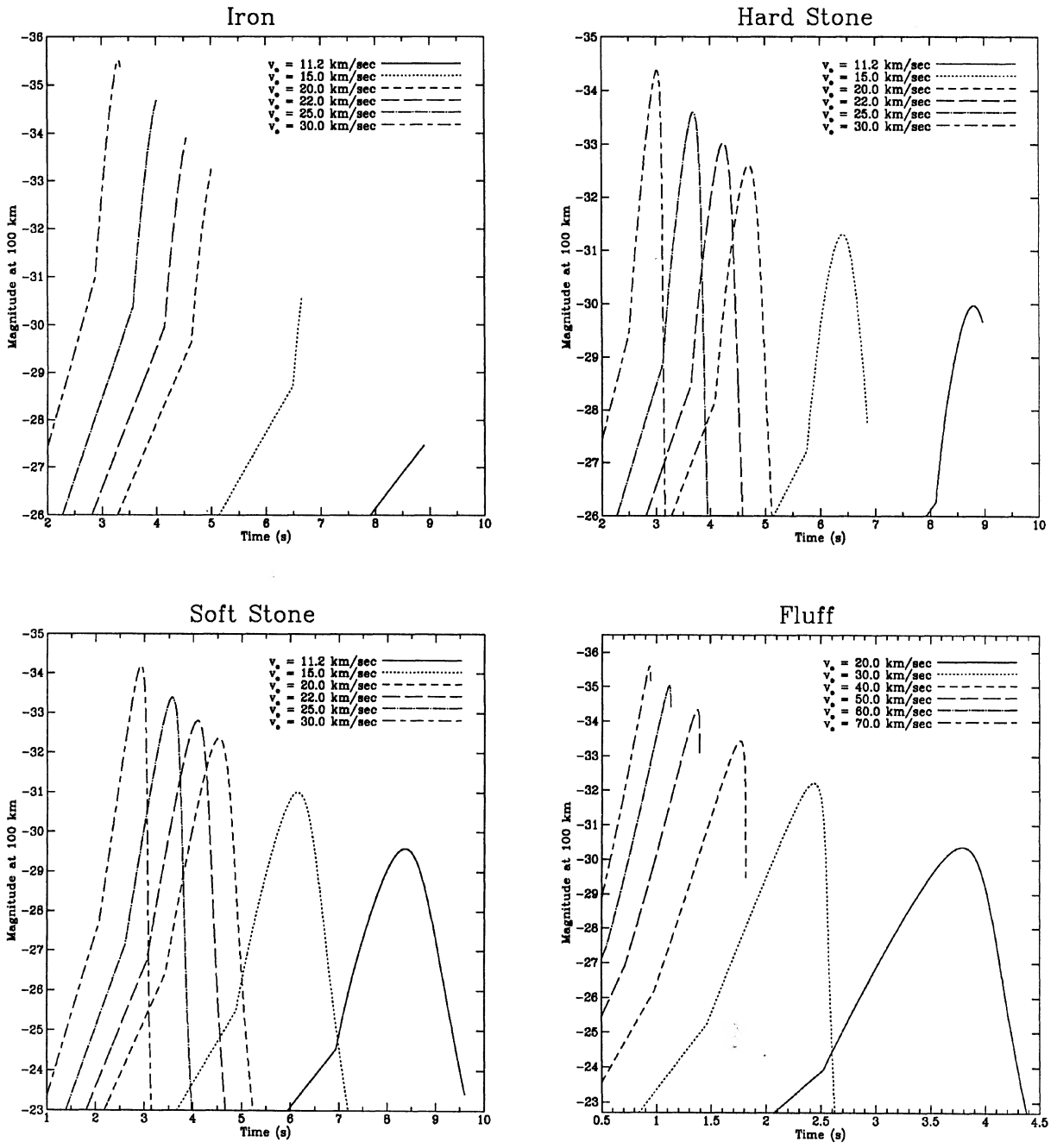

FIG. 7. The absolute visual magnitude of the meteors of the impactors shown in Figs. 1 and 2. These are given as a function of the elapsed time since the objects entered the atmosphere at a height of 100 km. Here the absolute magnitude is the apparent magnitude as observed at 100 km. The radius of each impactor is 50 m.

Tunguska impactor, which was −31.9 to −30.5 (Sekanina 1983), which indicates that the radius of the Tunguska impactor may have been a little smaller than 50 m.

Figure 8 shows the peak visual magnitude of impactors as a function of their radius for various impact velocities and composition types. The inflection point in the left (lower mass) side of each figure occurs when the objects are just big enough to fragment in the atmosphere. The inflection point on the right side of the graph occurs when the object is sufficiently massive that it hits the ground with most of its original kinetic energy. For objects to the right of this second inflection point, the peak luminosity in the air occurs just before the object impacts the ground. We see that if the Tunguska impact had an absolute magnitude of −31.2 and an impact velocity of about 20 km/s, its radius was about 40 m, but the uncertainty in its magnitude is

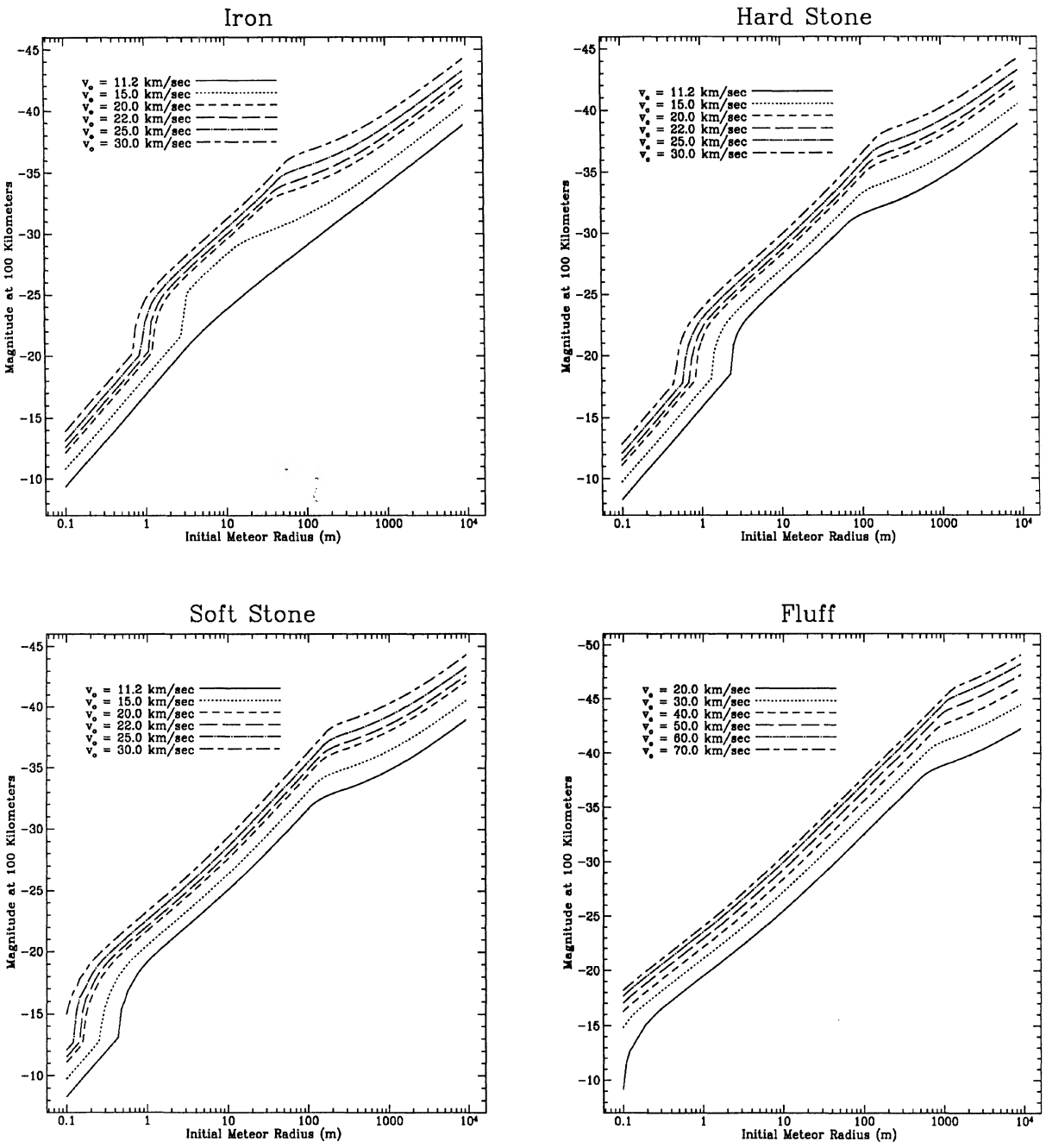

FIG. 8. The peak absolute visual magnitude of impactors as a function of their radii. This is computed for various impact velocities for the composition types given in earlier figures.

consistent with a radius of 30 to 50 m. This result is not very different if we had used the hard stone rather than the more common soft stone, so this result is not very sensitive to the material strength S of the stony meteoroid.

3.3 Debris Pattern and Impact Velocity at the Ground

Figure 9 shows the expansion radius, r_{exp}, of the debris pattern as a function of impactor radius for various impact velocities. Here $r_{exp}=(r_g-R_0)$ where r_g is the radius of the debris pattern on the ground and R_0 is the initial radius of meteoroid. If the meteoroid does not fragment, then we require that $r_{exp}=0$. If it fragments, r_g is taken to be its radius, r_d as given by Eq. (12) at the time when fragmentation stops or the debris hits the ground. This procedure will underestimate r_{exp} for small meteoroids that only go through a few stages of fragmentation and stop fragmenting well above the ground.

We note that r_{exp} for large stone meteoroids, which start

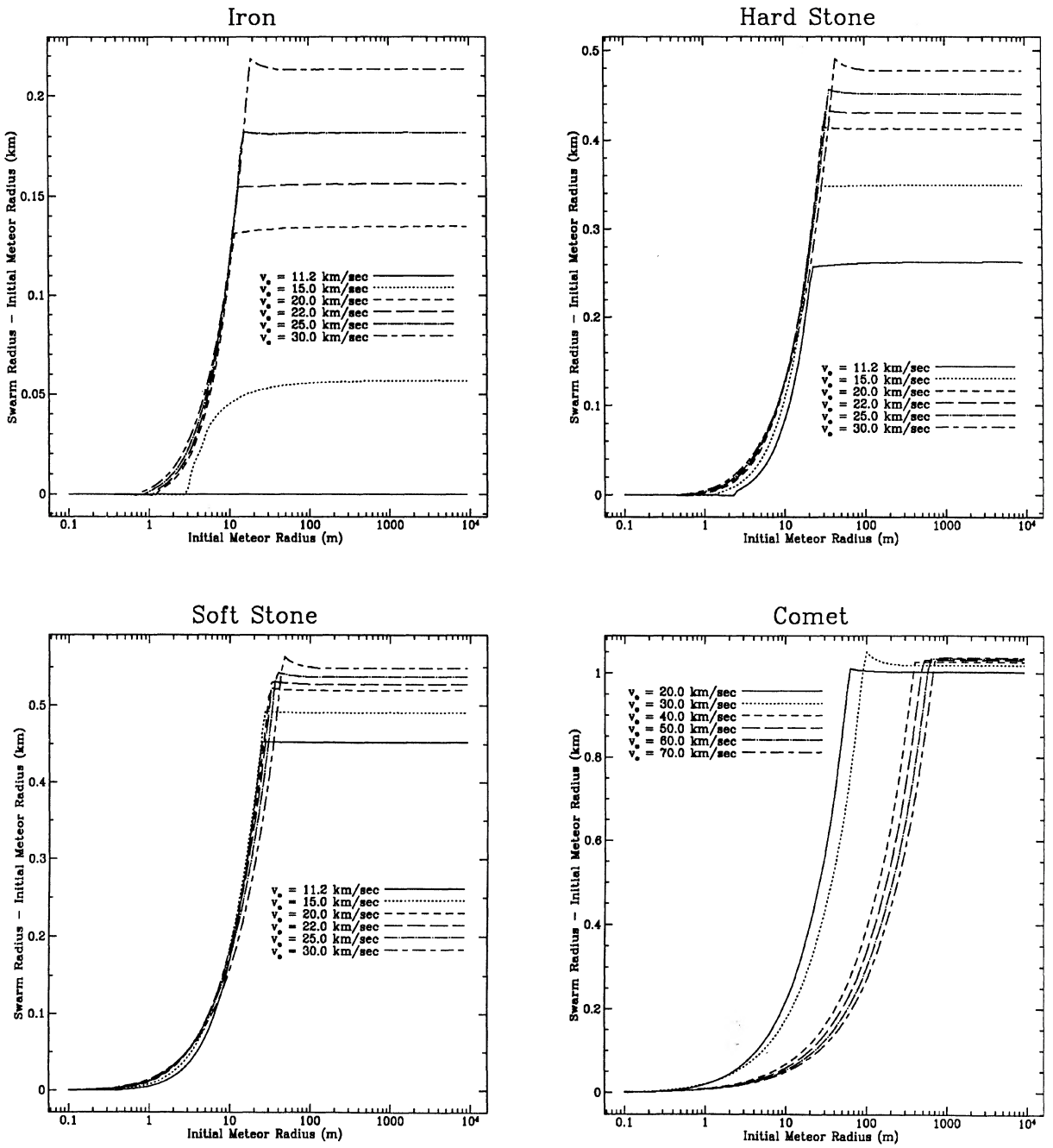

FIG. 9. The expansion radius, r_{exp}, of the debris as a function of the initial impactor radius. This is computed for various impact velocities and composition types. Here $r_{exp}=(r_g-R_0)$ where R_0 is the initial radius of the impactor and r_g is the radius of the debris when it hits the ground. If the object stops fragmenting before it hits the ground, r_g is taken as the radius of the debris pattern at the point where each subfragment acquires its own bow shock.

fragmenting well above the ground and continue fragmenting to ground level, approaches the value given by Eq. (15). Iron meteoroids fragment low in the atmosphere, so their r_{exp} is much less than R_{max}. We also note that r_{exp} increases with impact velocity because the breakup occurs higher up in the atmosphere.

Our calculations assume that asteroids have uniform material strength S. If they have large-scale cracks in them they could break apart along these cracks before their main structure begins to fail. This will produce a few pieces rather than a general fragmentation. These pieces, in turn, would develop their own bow shocks and undergo general fragmentation lower in the atmosphere where the ram pressure exceeds S. If these premature splittings occur very high in the atmosphere, they would produce a series of quasiindependent falls that may overlap.

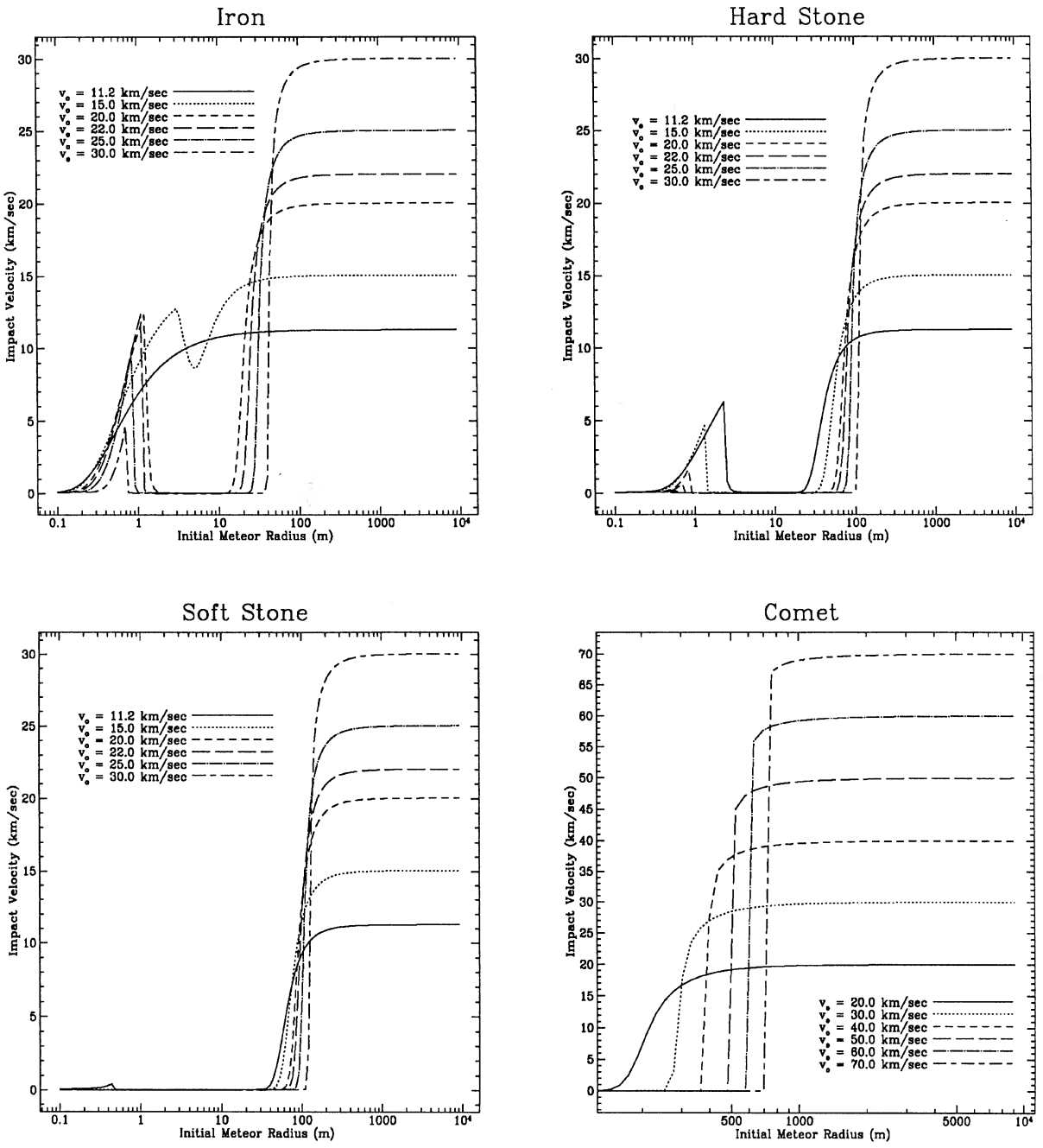

FIG. 10. The velocity at which the debris hits the ground. This is plotted as a function of impactor radius for various impact velocities and composition types.

Figure 10 shows the velocity at which the debris hits the ground. If the meteoroid fragments, but the fragmentation stops above the ground, the ground impact velocity is taken to be that of the largest fragment whose mass is determined by Eq. (2). The remaining debris will impact at a lower velocity. If fragmentation occurs, but it stops well above the ground, the debris is usually slowed to near terminal velocity (except for nickel–iron meteorites) at its impact with the ground.

Impacts by iron asteroids exhibit the most interesting structure in Fig. 10. We notice that nickel–iron meteoroids with initial impact velocities $V=11.2$ km/s do not fragment at any height h while those with $V=15$ km/s only break up at $h<3$ km. For $V=11.2$–15 km/s, the impact velocity with the ground increases from the terminal value for meteoroids with radii $R<0.1$ m to near the initial impact velocity V for those with $R>10$ meters. Fragmentation causes a local peak in the curve of about 12 km/s for

objects with radii of about 0.7–1 m and initial impact velocities of 20–25 km/s. Objects in the peak are large enough that they are not slowed severely by the atmosphere, but they are slowed enough to prevent their fragmenting. The peak impact velocity approaches the value of V_{max} given by Eq. (7).

We note that impactors with initial velocities of 30 km/s peak at a lower impact velocity of about 4 km/s. This is a result of their higher velocity dissipation in the atmosphere that results from their fragmenting higher in the atmosphere. These objects only undergo a few fragmentations before they are slowed enough that they cannot fragment further. Objects with radii slightly larger than those at the peak velocity have more mass per unit area than those at the peak, which causes them to continue fragmenting longer, which results in their fragmenting into much smaller pieces that quickly decelerate, so they have small impact velocities. Nickel–iron meteorites with radii exceeding 10 m impact the ground at near their initial velocities.

Stony meteorites also have a secondary hump in the ground impact velocity. This peak velocity is much reduced compared to that for iron, as one would expect from Eq. (7). Stones hit the ground at their initial velocities for radii exceeding about 100 m. A typical comet with an impact velocity of 40 km/s hits the ground at its impact velocity if its radius exceeds 500 m.

3.4 Largest Meteorite Fragments

Figure 11 shows the mass of the largest fragment given by Eq. (2) for stony and iron meteorites. The fact that no nickel–iron meteorites have been found with masses greater than about 50 metric tons is likely the result of impact erosion for low-velocity impactors and the result of fragmentation for the higher velocity ones.

Iron meteoroids with initial velocities in the range $V=11.2$ km/s to V_{max} [where $V_{max}=12.4$ km/s by Eq. (7)] never attain the dynamic pressure needed for fragmentation, so they impact the ground with their initial mass minus the mass ablated off the surface. The initial radius of an iron meteoroid with an initial impact velocity within this range of V, which corresponds to an approach velocity of 0 to 5.4 km/s before the gravitational acceleration by the Earth, would have to be nearly 2 m if the mass of meteorite impacting the ground is to exceed 50 metric tons. Figure 10 shows that such an object impacts the ground at more than 9 km/s. Shock erosion is very significant at this velocity, even for steel penetrators (Nickolas & Recht 1990), so shock erosion is the factor limiting the mass of iron meteorites that do not fragment.

Iron meteorites of sufficient size will fragment if their initial impact velocities $V \geqslant V_{max}=12.4$ km/s. Fragmentation is enough to keep the largest mass of any fragment well below 50 metric tons if $V \geqslant 20$ km/s. We see from Fig. 11 that the sequential fragmentation that occurs for $V \geqslant 20$ km/s collapses the maximum size of any nickel–iron meteorite produced by meteoroids with initial radii between 1–2 and 10 m. The objects in this radius range fragment enough that they produce smaller meteorites than those with smaller initial radii that are able to decelerate enough in the upper atmosphere to avoid significant fragmentation. The effectiveness of this fragmentation is also illustrated in Fig. 5, which shows a rapid divergence for $R > 1$–2 m in the heights between where fragmentation first occurs and where it stops.

As we noted earlier, the Sikhote–Aline nickel–iron impactor of 1947 had an initial radius of about 2 m and an impact velocity of 18–22 km/s, which puts it at the boundary between those meteorites that can get through the atmosphere without fragmentation and those that suffer fragmentation. It fragmented, with the largest recovered meteorite being 1.7 tons, but it is likely that the fragments that produced the largest craters suffered considerable impact erosion. If it had been a little larger, it would have fragmented into a large number of much smaller pieces that would have dissipated nearly all their energy in the atmosphere, so there would have been less impact damage.

If nickel-iron meteorites have initial radii exceeding 10 m, they impact with most of their initial kinetic energy. They are also large enough that they do not have time to undergo very many stages of fragmentation before they impact the ground; i.e., the dispersal velocities of the fragments are independent of the size of the object for a given local velocity and atmospheric density, so the time required for the radius of the cloud of fragments to double is directly proportional to this radius. The long time required to dissociate the larger meteoroids is responsible for the increase in the size of the fragments for iron impactors with radii exceeding 10 m. However, these larger fragments hit the ground at nearly the original impact velocity of the meteoroid, so they will suffer severe, if not total shock erosion.

Large stones fragment even at the parabolic impact velocity of 11.2 km/s. The largest stony meteorites are produced by meteoroids that decelerate enough that they do not fragment (or fragment into a few pieces at very high altitude because of large-scale initial cracks). The mass of these meteorites goes up steadily with increasing mass of the initial object until fragmentation begins. However, Fig. 8 shows that V_g, their impact velocity with the ground, also increases up to the value of V_{max} given by Eq. (7).

Figure 11 shows that the mass of the largest soft (common) stone that is expected to hit the ground as a meteorite is under 1 metric ton even at the parabolic speed, which is in agreement with observations. Hard stone meteorites impacting at $V=11.2$ km/s, can produce impacting (unfragmented) objects with masses up to 100 metric tons, but we see from Fig. 10 that these objects impact the ground at about 7 km/s, which would certainly destroy any rock. A surviving hard stone meteorite with a mass of 1 metric ton, has a ground impact velocity of about 4 km/s. For hard stones, the mass of the largest surviving meteorites is primarily limited by shock erosion.

Fragmentation causes a collapse in the mass of the meteorites produced by stony impactors of intermediate size, as it does for the iron impactors. Figure 11 shows that the Tunguska impactor, which had an initial radius of about 40 m and $V \geqslant 20$ km/s, is expected to have produced frag-

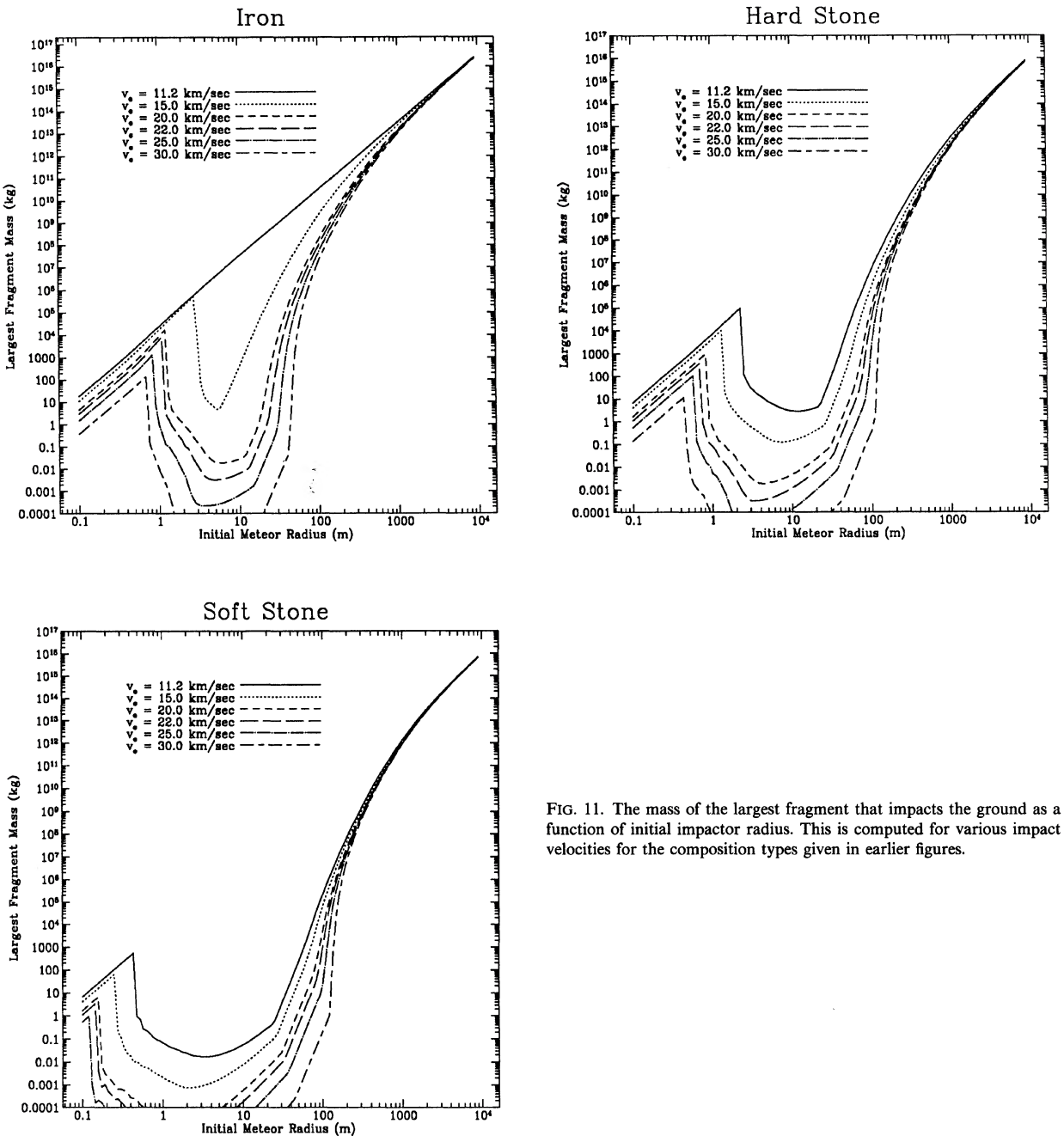

FIG. 11. The mass of the largest fragment that impacts the ground as a function of initial impactor radius. This is computed for various impact velocities for the composition types given in earlier figures.

ments with a maximum mass of less than 1 kg=0.001 metric ton! It is clear why no large meteorites have been found from this fall. We also note from the work in the previous section that this pile of gravel is likely to be confined to an area of about 2–3 km^2, which is much smaller than the 2000 km^2 of forest that was destroyed by the fall. If the debris is dispersed over a radius of 1 km, its average depth would be less than 10 cm, if we ignored ablation losses. At 20 km/s, about 90% of the mass is ablated, so the layer is likely to be less than 1 cm thick.

The mass of the largest fragment hitting the ground begins to increase rapidly for still larger stony meteoroids because the objects to do not have time to go through many stages of fragmentation before they hit the ground. This was obviously the case for the impactor producing the Rio Cuarto Crater Field in Argentina (Schultz & Lianza 1992). This grazing impactor divided into a few large fragments. The structure of the impact craters indicates that each of these fragments was fractured into a number of still smaller fragments. The initial radius of this object was up to 150 m, which Fig. 11 shows would produce fragments with maximum masses between 10^6 to 10^7 metric tons, or about 2.5% to 25% of the mass of the original fragment. Such large fragments hit the ground at nearly the initial

impact velocity, so very little of their mass survives shock erosion. The craters they produced are their only fossils.

3.5 Damage Done by the Impact

Knowing the damage done by impactors is both interesting in assessing the effect of future asteroid–comet collisions and in finding signatures of impactors that may be identified in the geological record of the Earth.

3.5.1 Pressure pulse in the atmosphere

Even if all the meteoroid energy is dissipated in the atmosphere, the impact can cause considerable ground damage due to the atmospheric blast wave; e.g., the Tunguska impactor of 1908 devastated an area of 2000 km^2 without producing an impact crater (Sekanina 1983).

We saw in Figs. 2 and 3 that most of the atmospheric energy dissipation occurs in a narrow range of height around $h_{\rm half}$, the half-energy height. This allows us to approximate the energy release as a point explosion at $h_{\rm half}$. There is much experimental data from the 1940's and 1950's on the effects of nuclear explosives fired at various heights and yields. Johndale Solem (Theoretical Division, LANL) finds from this data that the outer radius r_4 at the ground below the point of detonation at height h where the over pressure due to the atmospheric airburst exceeds 4 psi$=2.8\times10^5$ dynes/cm^2, which is enough to knock down trees and economically destroy most buildings, can be approximated by the fitting formula

$$r_4=ah-bh^2E^{-1/3}+cE^{1/3}, \tag{39}$$

where $a=2.09$, $b=156$ erg$^{1/3}$/cm and $c=0.0146$ cm/erg$^{1/3}$. For r_4 and h in km and E in Mtons (Megatons of TNT$=4.2\times10^{22}$ ergs), $a=2.09$, $b=0.449$, and $c=5.08$. [Similar results, in less convenient form, may be found in Glasstone & Dolan (1977, Chap. 3).] (Determining r_4 directly from theory is difficult because it depends on an interplay between the shock propagating directly from the point of energy release and that reflected from the ground, the Mach effect.)

This empirical formula is believed to be highly accurate for heights less than 65 km and yields less than 1 gigaton $=1000$ megatons$=4.2\times10^{25}$ ergs. For yields larger than this value, the curvature of the Earth is important. Energies above a gigaton are large enough to blow off most of the atmosphere along the line of site, so a yield above a gigaton would simply blow off the atmosphere at a higher velocity, but it would do no more damage to the rest of the atmosphere than would a lower yield event. Stony meteorites with a typical velocity of 20 km/s exceed this energy if their radii exceed 120 m. An impactor of this size or larger is not likely to leave any surviving witnesses because of the ejection of all the atmosphere along the line of site. It would also produce enormous afterwinds in the region around this blowout hole as the atmosphere rushes in to refill it. This filling in and the subsequent rebound produces a pressure pulse that propagates around the world.

Equation (39) indicates that for a given yield, there is critical height, h_c, above which no ground damage (at 4 psi) or greater occurs. This occurs at a height

$$h_c=\frac{a}{2b}\left[1+\left(1+\frac{4bc}{a^2}\right)^{1/2}\right]E^{1/3}=6.42\ \text{km}\left(\frac{E}{\text{Mtons}}\right)^{1/3}. \tag{40}$$

We also find from Eq. (39) that the "optimum" height at which radius of destruction is a maximum for a given yield E is

$$h_{\rm opt}=\frac{a}{2b}E^{1/3}=2.33\ \text{km}\left(\frac{E}{\text{Mtons}}\right)^{1/3}=0.36h_c. \tag{41}$$

The maximum radius of destruction for an explosion occurring at this "optimum" height is

$$r_4=\left(\frac{a^2}{4b}+c\right)E^{1/3}=7.5\ \text{km}\left(\frac{E}{\text{Mtons}}\right)^{1/3}. \tag{42}$$

This is 1.48 larger than the radius of destruction achieved if the energy release occurs at $h=0$.

The kinetic energy of the asteroid is given by

$$E=\frac{1}{2}MV_0^2$$

$$=75\ \text{Mgtons}\left(\frac{\rho_{\mathcal{M}}}{3\ \text{g/cm}^3}\right)\left(\frac{R}{50\ \text{m}}\right)^3\left(\frac{V_0}{20\ \text{km/s}}\right)^2. \tag{43}$$

Figure 12 shows the radius of destruction derived from Eq. (39) as a function of impactor radius for various compositions and impact velocities. For h in Eq. (39) we used $h_{\rm half}$, the height at which half the energy was dissipated. Here we have also assumed the energy dissipation occurs at sea level ($h=0$) if less than half of the energy was dissipated before the meteorite hit the ground. We have also assumed that all the kinetic energy is dissipated in the atmosphere, which is clearly not the case if the object hits the ground at nearly its initial velocity.

We see from Fig. 12 that the blast waves from soft stony meteorites, which constitute about 95% of the total meteorites, only cause ground damage if their radii exceed about 28 m. For $V=20$–25 km/s, the radius of destruction increases very rapidly with asteroid radius reaching the area of Chicago for $R=34$ m.

There has been some controversy about the nature of Tunguska impactor (Sekinina 1983), but Fig. 12 shows that its area of destruction is consistent with a soft stony meteoroid with a radius of about 40 m ($V=22$ km/s), and a probable impact energy of about 48 Mtons. We saw earlier that the observed peak brightness was also consistent with an object of this size. Extrapolations from the statistics of more massive Earth-Crossing asteroids (ECAs) suggests that a Tunguska size (for $D=2R=80$ m) impactor hits Earth about every 100 yr (Shoemaker *et al.* 1990).

The radius of destruction continues to increase rapidly with increasing asteroid radius. A stony asteroid with a radius of 150 m, which is about the size of the one that produced the Rio Cuarto crater field in Argentina, would wipe out (at 4 psi or greater) an area the size of Connecticut or larger. This would have an impact energy of about 2 Gtons$=2000$ Mtons with most of this energy being dissipated after the fragments hit the ground. An object of

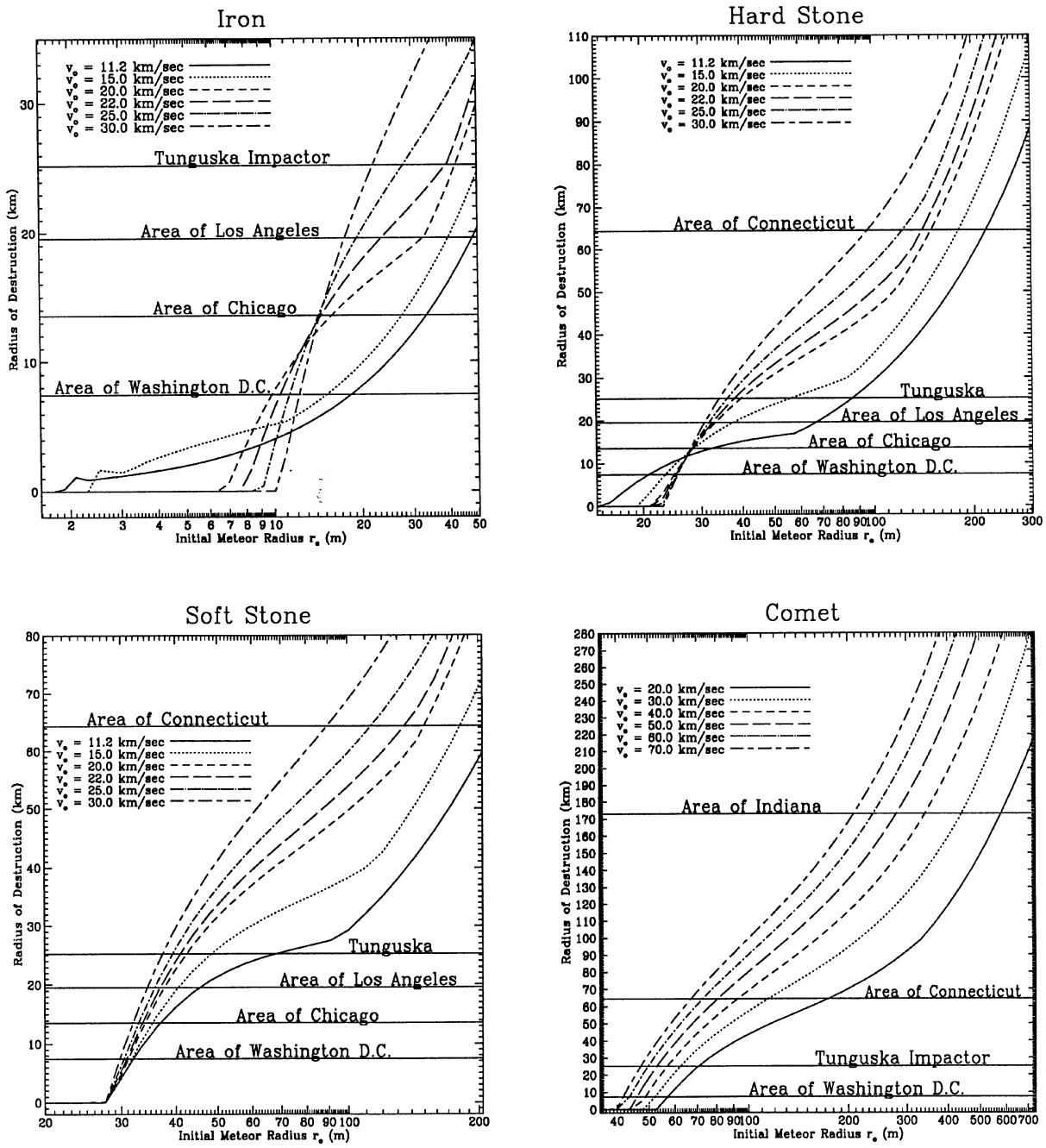

FIG. 12. The radius of destruction around the impact point due to the atmospheric blast wave. This is defined to be where the overpressure is at least 4 psi $=2.8\times10^5$ dynes/cm^2, which is enough to knock down trees and economically destroy buildings.

this size hits the Earth about every 3000 yr. The Rio Cuarto impactor fell "considerably less" than 10 000 years ago (Shultz & Lianza 1992), after humans reached the Americas.

We see from Fig. 12 that the blast damage from nickel–iron asteroids begins at a much smaller radius than for stones. This is largely due to iron meteoroids fragmenting and dissipating their energy at much lower h. They are also nearly three times denser than stone, so they have nearly three times as much kinetic energy for a given radius. Figure 12 shows that nickel–iron meteoroids with radii $R>2$ m cause ground damage if $V_0=11.2$ km/s, the lowest (parabolic) velocity available to a meteorite hitting the earth. The minimum R for ground damage increases to 10 m for $V_0=30$ km/s due to the fragmentation and energy dissipation occurring higher in the atmosphere.

Comets with typical impact velocities of 40 km/s cause ground damage if their radii exceed 50 m. One 300 m in

radius would destroy an area nearly the size of Indiana. This may overstate, somewhat, the area of destruction because the maximum area of destruction due to the blast-wave cannot exceed the line-of-sight distance to the comet (except for the afterwind that fills in the atmospheric hole). The line-of-sight distance is large because a comet dissipates its energy high in the atmosphere.

Because it takes a smaller iron impactor than a stony one to produce a given amount of damage, the fraction of damaged regions of a given size that are produced by iron impactors is much larger than the fraction of asteroids of fixed size that are irons. Part of this arises from the higher density of iron asteroids and their fragmenting lower in the atmosphere and part is due to the rapid increase in the number of asteroids with decreasing radius. The relative frequency of all asteroids in some range of radii $(R \pm \Delta R)$ scales as R^{-4}. The fraction of the damaged regions of a given size that are produced by iron impactors is given by

$$F_i = \left[\frac{f_i \left(\frac{R_s}{R_i} \right)^4}{f_i \left(\frac{R_s}{R_i} \right)^4 + f_s} \right]. \quad (44)$$

Here R_s is the radius of a stone meteoroid that is required to produce a given amount of damage and R_i is the radius of an iron meteoroid that is required to produce the same damage. Here f_i is the fraction of meteoroids of a fixed radius that are iron and f_s is the corresponding one for stones. We shall assume that $f_i = 0.05$ and $f_s = 0.95$. As an example of the application of Eq. (44), we note that to destroy an area comparable to that of Chicago requires a nickel–iron meteorite with a radius of $R_i = 15$ m and a stony meteorite with a radius of $R_s = 33$ m if the impact velocity is 22 km/s. We find that the fraction of the impactors producing an area of destruction comparable to that of Chicago that are iron meteorites is about $F_i = 0.55$. For Washington, DC $F_i = 0.80$. In the limit where the impactors are large enough that they hit the ground before dissipating most of their energy, the relative fraction of irons among those impactors that produce a given amount of damage is about $F_i = 0.185$, due to the higher density of the irons.

Figure 13 shows r_4, the radius of destruction, in units of what it would be if all the kinetic energy is released at $h = 0$. We see that the maximum radius of destruction is about 1.5 times larger than that produced by a ground burst of the same energy, so the area of destruction is more than twice as large. We see that the fragmentation and atmospheric dissipation of soft stony asteroids with radii in the range of 35 to 160 m and typical impact velocities of 22 km/s produce more airblast damage than if all their energy had been dissipated at sea level. This includes objects ranging from the Tunguska impactor to the Rio Cuarto impactor.

3.5.2 Fires from the radiation flux

The trees at Tunguska were charred, but there were no large-scale fires (Sekanina 1983). However, there were massive fires associated with the Cretaceous–Tertiary Impactor (Wolbach *et al.* 1985).

Fires or charring are likely produced by the radiation load from the meteor. It is known from work on nuclear weapons (Glasstone & Dolan 1977) that pine forests will catch on fire if the radiation load exceeds about 10 cal/cm^2 $= 4.2 \times 10^8$ ergs/cm^2. Deciduous forests catch fire at about half this radiation load.

The radiation load (ergs/cm^2) at a distance S from the ground impact point of a meteor coming in at zero zenith angle is given by

$$F = \int_{100\ \mathrm{km}}^{0} \left(\frac{L}{4\pi h^2} \right) \left[1 + \left(\frac{S}{h} \right)^2 \right]^{-3/2} \frac{dh}{V}. \quad (45)$$

We assume that L is the optical luminosity given by Eq. (37), although the infrared and near-UV will contribute to the radiation load. More energetic UV will also be felt after the meteor passes through the ozone layer. We also ignore atmospheric absorption, which will reduce the radiation load, and we ignore the curvature of the Earth. Figure 14 shows the radiation load at a distance $S = 10$ km for iron and stony meteorites and $S = 50$ km for comets (which dissipate much higher in the atmosphere and light up a larger area).

The radiation load from a soft-stone asteroid is enough to ignite pine forests out to 10 km if $R \approx 40$ m (the radius of the Tunguska impactor). However, we see from Fig. 12 that the blast wave from such an impactor would extend out to 25 km. Experimental work on the effects of nuclear weapons (Glasstone & Dolan 1973) showed that the prompt radiation from a nuclear weapon would often char buildings and start them burning, but the arrival of the airblast would blow them out. We expect the same thing to have happened during the impact of the 40-meteor radius Tunguksa asteroid. It would set the forest on fire, but the airblast would blow it out. This evidently happened at Tunguska where the trees were charred, but no fires were started. Very large asteroids coming at large zenith angles may be able to start fires and then impact over the horizon where the blast wave and the afterwind produced by the filling in of the atmospheric hole may not be able to put out the fires, but this is an unlikely event.

Comets start fires more easily than asteroids. They dissipate their energy much higher in the atmosphere, which allows them to illuminate a much larger area of the Earth. The high-altitude energy dissipation makes it more difficult for the atmospheric shock waves to reach the surface of the earth. To produce fires 50 km from the impact point requires a comet with a radius of 100 m if the impact velocity is 50 km/s. Such a comet would produce a 4 psi blast wave out to about 80 km from the impact point. While this is 1.6 times larger than the radius in which fires are started, it is much smaller than the ratio of 2.5 found for the stony meteorites. In addition, because of the high altitude at which the comet dissipates its energy and the larger length scales involved, the fires will have burned much longer for

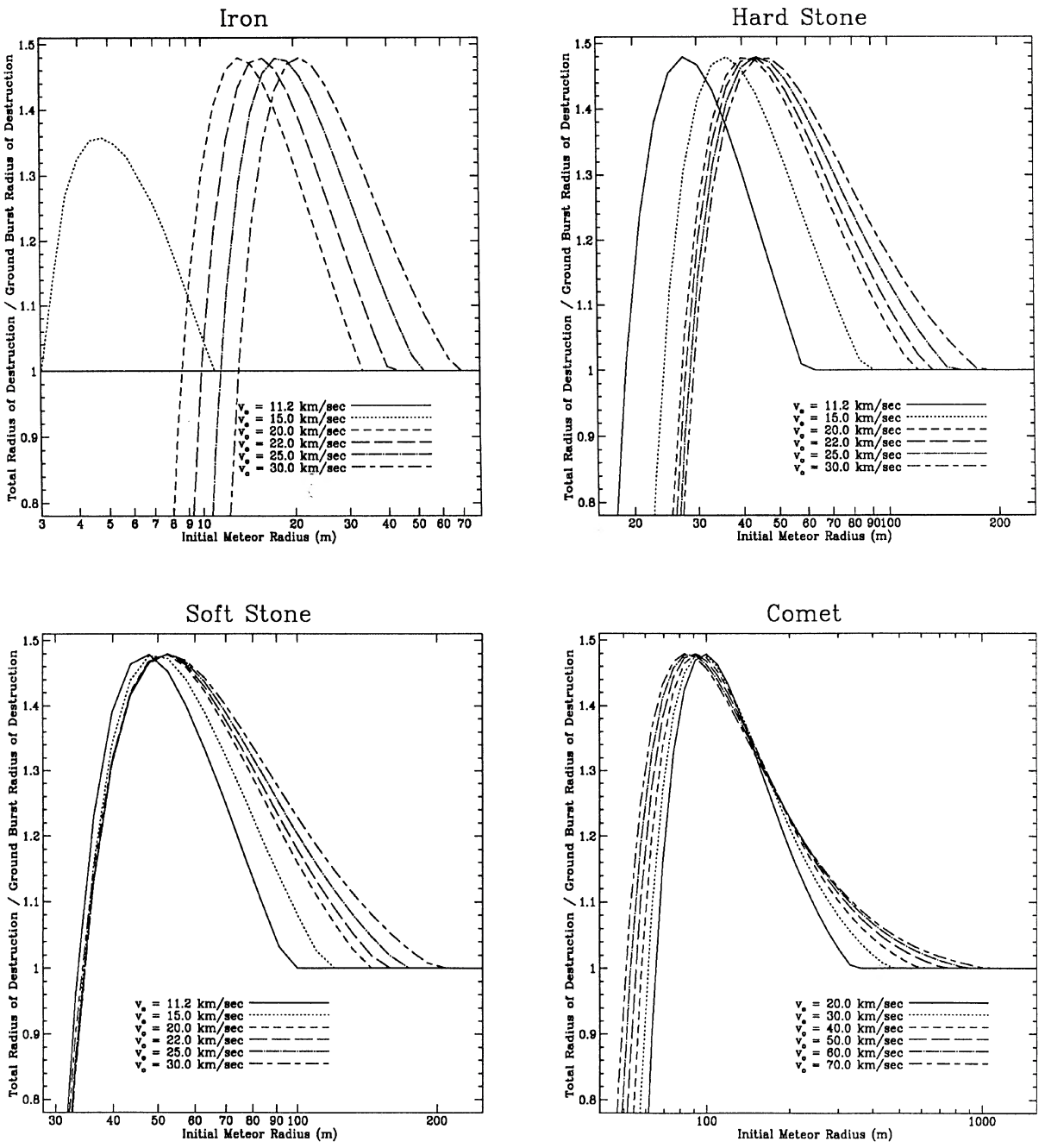

FIG. 13. The radius of destruction given in Fig. 10 in units of what it would be if the same amount of energy had been released at ground level, $h=0$.

a comet than for an asteroid impact before the blast wave or afterwind reaches the fires. The fire may have burned for a sufficiently long time when the blast or afterwind arrives that while it may blow out momentarily, it would reignite shortly after the disturbance passes. The bigger the impactor, the longer the mean delay between the time the fire starts and the arrival of the blast wave or afterwind, so bigger impactors are more likely to start fires than smaller ones.

The fact that the Cretaceous–Tertiary impactor produced widespread fires suggests that it was a comet rather than an asteroid. A fire several hundred kilometers across is hard to imagine. It would produce large-scale currents that would feed it new oxygen. It is not difficult to see how it might spread over an entire continent, which is what is required to explain the total biomass burned in the Cretaceous–Tertiary event (Wolbach *et al.* 1985).

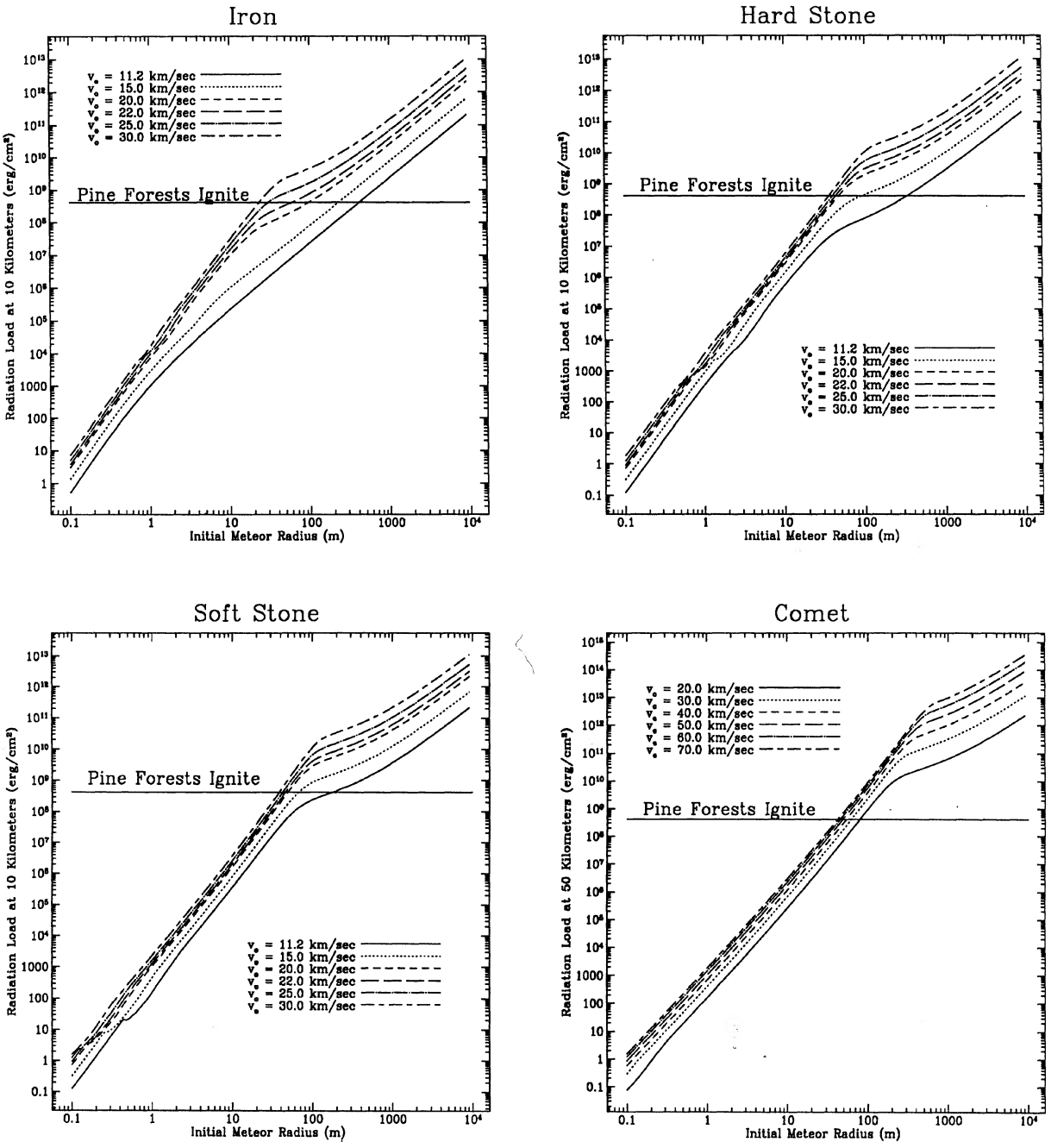

FIG. 14. The radiation load (in erg/cm^2) at 10 km from the impact point for asteroids and 50 km away for comets. This is given as a function of impactor radius for various impact velocities and composition types.

3.5.3 Global dust distribution

The Cretaceous–Tertiary impactor deposited a layer of dust about 2 cm thick around the Earth (Alvarez *et al.* 1980). If it is composed of grains 1 μm$=10^{-4}$ cm in diameter, the optical depth through this layer is about $\tau=10^4$. This dust was in the atmosphere at one time, and it took some weeks if not months to settle. It is this image of total darkness for a protracted period of time that has mesmerized the research community concerned with the effects of the killer asteroid (or comet).

If some source (nuclear, asteroid–comet impact, or volcanic) puts more than about 150 megatons$=0.15$ gigatons $=6.3\times10^{24}$ ergs into the atmosphere, this hot bubble of gas does not reach pressure equilibrium at any height in

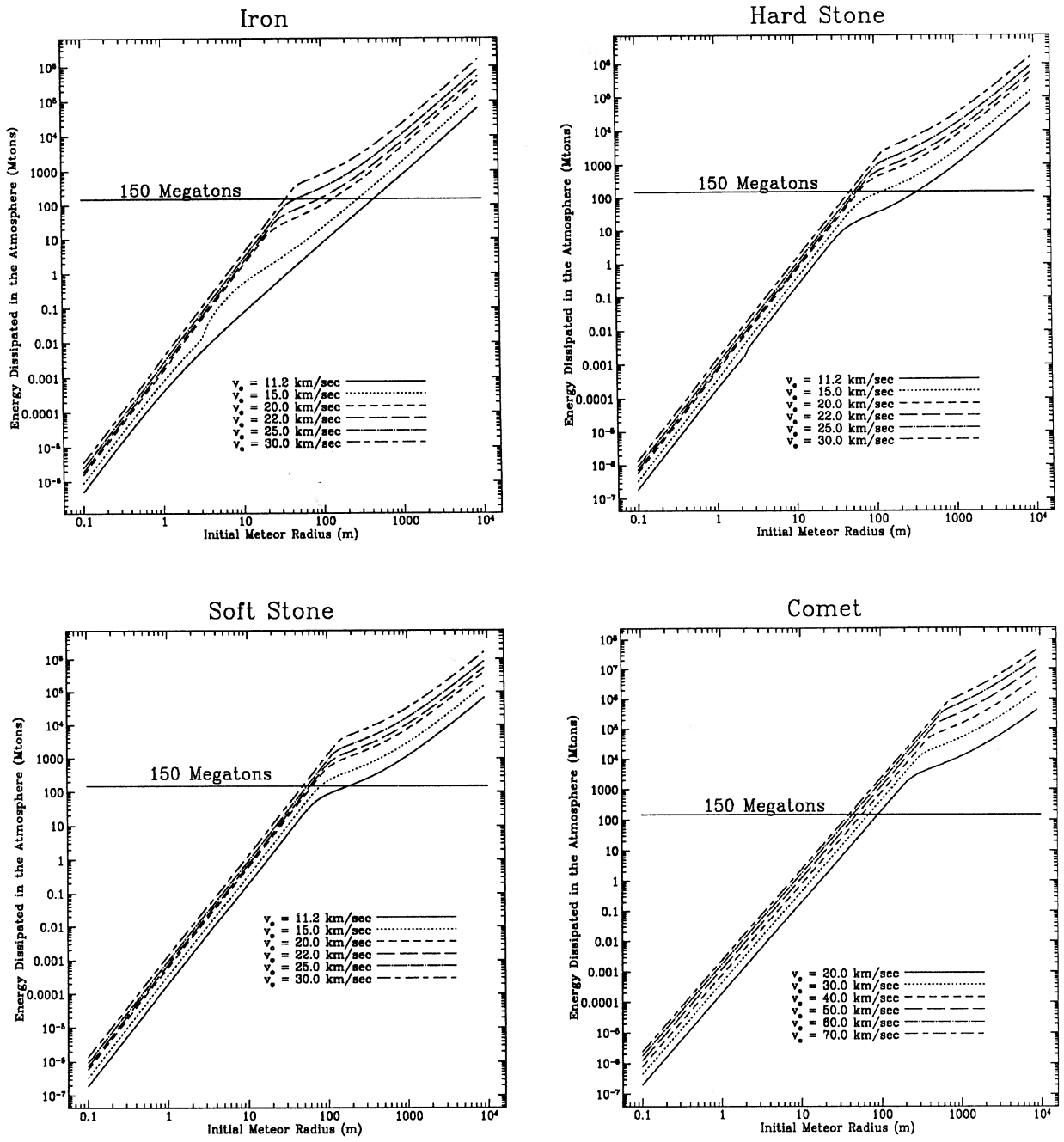

FIG. 15. The energy deposited into the atmosphere during the passage of an impactor as a function of its radius and impact velocity for the various composition classes.

the atmosphere (Jones & Kodas 1983). The classical mushroom-shaped (toroidal) cloud continues rising by buoyancy. It becomes larger as it rises until its diameter exceeds the scale height of the atmosphere. It is then no longer confined by the atmosphere, but it spreads out laterally to form a new high-entropy layer at the top of the atmosphere. Any dust entrapped in this gas will quickly spread uniformly around the Earth and settle out slowly by diffusion.

An asteroid or comet impact that releases more than 150 megatons in the atmosphere will produce a uniform global concentration of dust. Even though this dust layer may be too thin to produce a mass extinction, it could be thick enough to be detected in snow deposits in Greenland or Antarctica, so these deposits could potentially prove to be counters for large impactors of the past few hundred thousand years.

Figure 15 shows the energy that an impactor deposits in

the atmosphere before it hits the ground. (Some fraction of the energy at which it impacts the ground also goes into the air, but most of it goes into forming a crater. The ground is much more effective in soaking up the momentum of the impacting object than is the air because of its much larger density. For ordinary (soft) stony meteorites, the critical minimum radius of an asteroid that deposits this much energy into the atmosphere is about 60 m. An impactor this size or larger hits Earth about every 350 yr. (This radius can be found analytically, since stony meteoroids with radii less than 100 m deposit most of their energy in the atmosphere).

If the impactor loses most of its energy high above the ground, the only dust it can bring to the top of the atmosphere is its own mass. If the object impacts the ground with most of its initial velocity, the mass of the dust ejected may be several times that of the impactor. The afterwind that blows into the atmospheric hole left by the blast can carry a tremendous amount of dust to high altitude in nuclear explosions. It may be much more effective for asteroid–comet impacts because they can be much more energetic than any nuclear explosion.

If we assume that all of the impactor mass (for $R > 60$ m) forms a dust layer at the top of the atmosphere, its optical depth is

$$\tau = \frac{(R/a)^3 \pi a^2}{4\pi R_\oplus^2} = \frac{1}{4}\left(\frac{R}{R_\oplus}\right)^2 \frac{R}{a} = 0.0062\left(\frac{R}{100\ \text{m}}\right)^3 \left(\frac{\mu\text{m}}{a}\right), \quad (46)$$

where a is the mean radius of the grains and R is the impactor radius. If $R > 100$ m, most of the energy is dissipated on impact with the ground, which may increase the dust concentration in the atmosphere and its optical depth several fold. If only the mass of the impactor is available, then $R = 0.5$ km for $\tau = 1$, $R = 1.2$ km for $\tau = 10$, and $R = 11.8$ km for $\tau = 10^4$ (the Cretaceous–Tertiary dust layer). If the dust ejected is ten times the mass of the asteroid, this would only reduce the minimum radius of the asteroid needed to produce a given τ by a factor of 2. It is likely that an asteroid with a radius of at least 0.3–0.5 km is needed to produce significant darkening (cooling) of the entire earth. Such an impact should occur about every 10^{4-5} yr.

3.5.4 Craters

The diameter of a crater produced by a meteor impact (or nuclear explosion) of energy Y is given by the equation

$$D_{\text{crat}} = \left(\frac{Y}{0.952\ \text{Mton}}\right)^{1/3} \text{km}. \quad (47)$$

(Allen 1973). Figure 16 shows the crater radius $R_{\text{crat}} = 0.5$ D_{crat} computed by this equation based on the ground impact energy of the asteroid debris.

If fragmentation occurs, a single coherent crater will only form if $R_{\text{crat}} > r_d$, the radius of debris circle at the ground. Comparing Fig. 16 to Fig. 9, we see that for (soft) stony asteroids $R_{\text{crat}} > r_d$ only if the meteoroid radius $R > 50$ m for impact velocity $V = 11.2$ km/s and $R > 100$ m if $V = 30$ km/s. For iron meteorites $R_{\text{crat}} > r_d$ only if $R > 10$ m for $V = 20$ km/s and $R > 40$ m for $V = 30$ km/s. Iron meteorites with velocities of 11.2 to 12.4 km/s, do not fragment (unless they have pre-existing large-scale cracks), so they impact in one piece and form one coherent crater for all asteroid radii.

Small asteroids that fragment, but have $R_{\text{crat}} < r_d$, so they do not have enough total impact energy to form a coherent crater, will produce a shotgun-like pattern in a crater field with radius on the order of r_d. Figure 17 shows the radius of the crater produced by the largest fragment. The mass of this fragment is taken to be the post-ablation mass of the asteroid if it does not fragment and the mass given by Eq. (2) if it does fragment. We note the very sharp drop in crater size when the meteoroid becomes large enough to fragment. Only low-velocity iron impactors never fragment. All iron impactors with $V \geqslant V_{\max}$ and all stony asteroids fragment when their initial radius exceeds a certain value due to their not slowing down enough in the upper atmosphere to avoid the ram pressures that produce structural failures.

For stony and iron meteorites, there is range of initial meteoroid radii where the objects are large enough to hit the ground with enough speed to form craters, but they are small enough to have slowed enough that they suffer no fragmentation or only one level of fragmentation. The iron meteorite that stuck near the Russian town of Sterlitanak on 17 May 1990 (Petaev 1992) apparently did not fragment. Its radius was estimated to be $R = 0.5$ m. It produced a crater with a radius of 5 m, which is close to predicted crater radius given by Fig. 17. The large Sikhote–Aline nickel–iron meteorite with $R = 2$ m may have suffered one level of fragmentation. The radius of its largest crater was 14 m (Fessenkov 1955). Figure 17 shows that this is a little less than the maximum crater size we would expect from a nickel–iron meteorite with $R = 2$ m. Larger objects are not slowed down enough by the atmosphere to avoid multiple fragmentations, so the mass of their largest fragment collapses, as reflected in the crater sizes; e.g., if the radius of Sikhote–Aline meteorite had been 3 or 4 m instead of 2 m, it would have produced much smaller impact craters, but the damage from its airburst would have been very much worse. For much larger asteroids, the radius of the fragment increases very rapidly with R. This results from very large asteroids taking a long time to double the radii of their debris cloud, so they cannot suffer many levels of fragmentation before they hit the ground.

As the radius, R, of the asteroid becomes large enough that its R_{crat} approaches r_d, the craters within the debris circle will overlap to form a continuous but shallow crater. The Rio Cuarto crater field in Argentina [Schultz & Beatty (1992) and Schultz & Lianza (1992)] may be such a field. This asteroid came in at very large zenith angle, so the craters lie on a line 30 km long and ($r_d =$) 2 km wide. If the impactor had come straight down, it is likely that the craters would have overlapped to form a single one. Many of the smaller craters are composed of a number of parallel

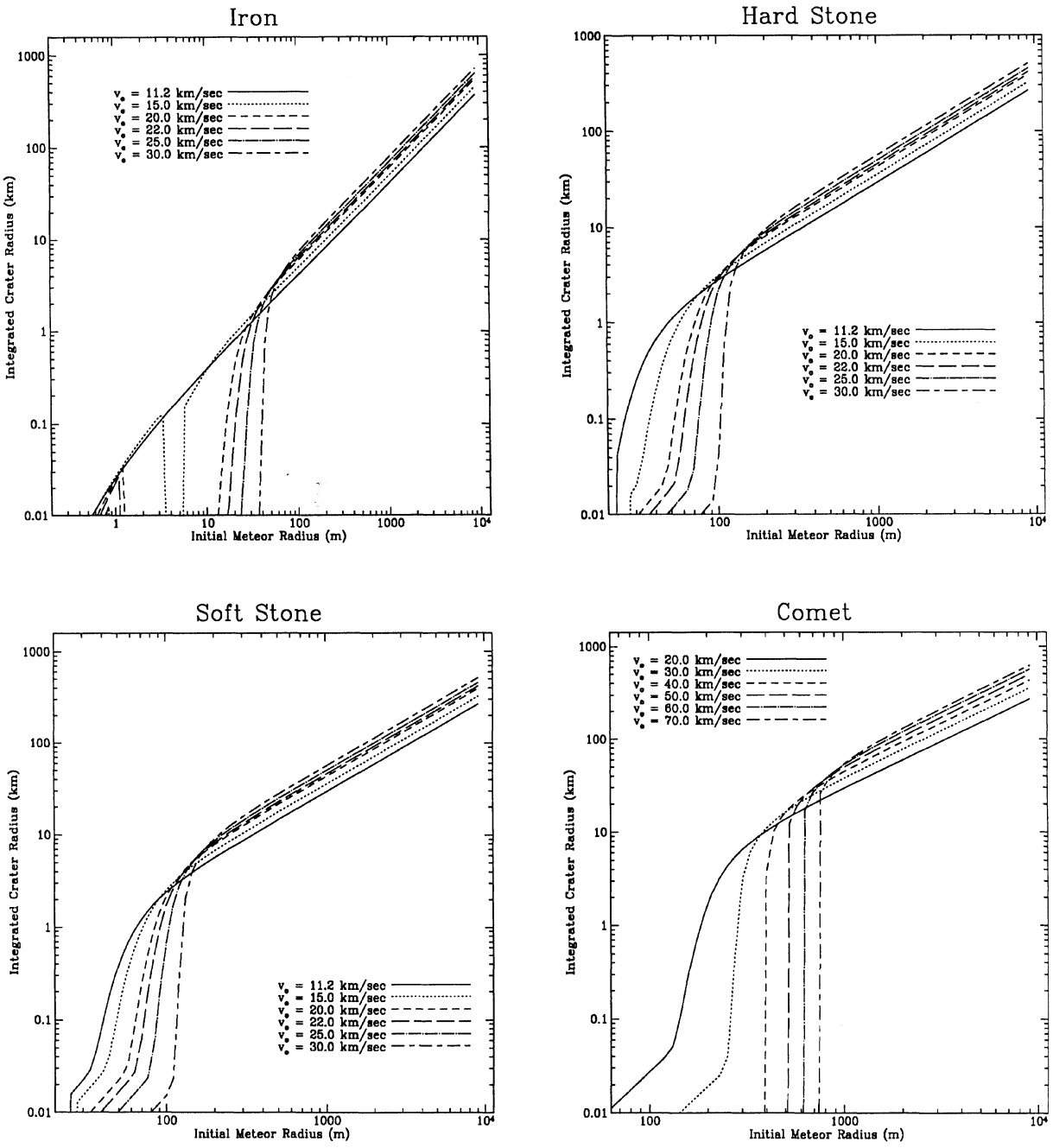

FIG. 16. The equivalent radius (in kilometers) of the crater produced if all of the impacting material (original mass after ablation) were collected into a single body that hits the ground at the impact velocity given in Fig. 8. This is given as a function of the original radius of the impactor for various impact velocities at the top of the atmosphere and for various composition classes.

overlapping craters indicating the progressive fragmentation of the original asteroid.

Figure 16 shows that the Barringer crater in Arizona with a radius of 620 m (Allen 1973), which exceeds r_d, may have been formed by a single nonfragmenting nickel–iron asteroid with a radius of 10 m and a velocity of 11.2–15 km/s. The Barringer crater is about 2 km above sea level, so even at $V=15$ km/s, there may have been no fragmentation or at least very little dispersal and slowing down of the fragments. It is less likely, but possible that the crater formed by the overlapping impacts of the fragments of an asteroid 20–30 m in radius that had an impact velocity of 20–30 km/s.

If the asteroid is large enough that it is not slowed significantly by the atmosphere, the diameter of the crater can be related to the initial asteroid radius R, density $\rho_{\mathcal{M}}$, and

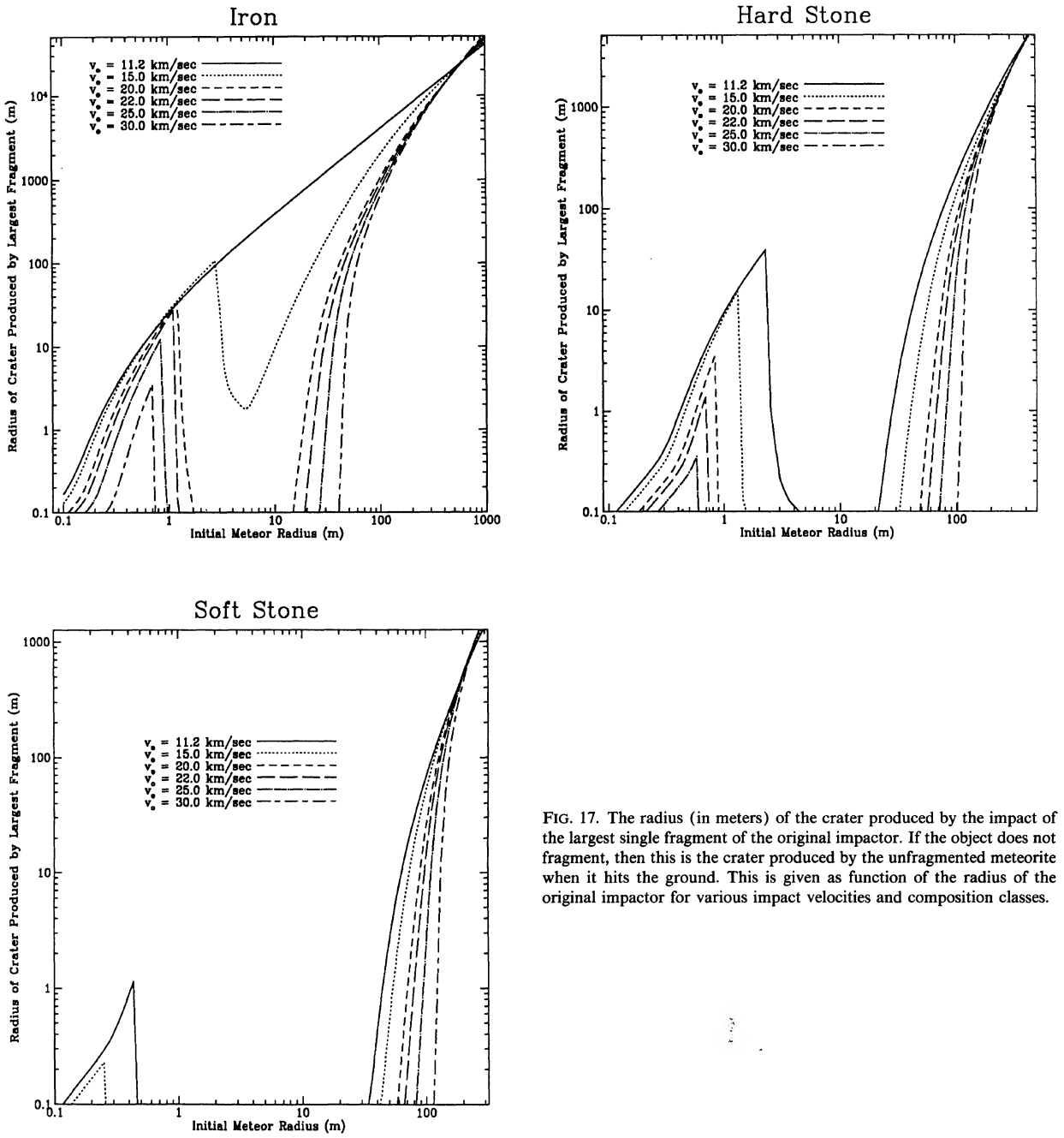

FIG. 17. The radius (in meters) of the crater produced by the impact of the largest single fragment of the original impactor. If the object does not fragment, then this is the crater produced by the unfragmented meteorite when it hits the ground. This is given as function of the radius of the original impactor for various impact velocities and composition classes.

impact velocity V of the asteroid by the equation

$$R_{\rm crat}=4.3\ {\rm km}\left[\left(\frac{R}{100\ {\rm m}}\right)^3\left(\frac{V}{20\ {\rm km}}\right)^2\left(\frac{\rho}{3\ {\rm g/cm^3}}\right)\right]^{1/3}. \quad (48)$$

This equation holds for stony meteorites with radii greater than about 100 m and iron ones with radii greater than about 20–30 m.

3.5.5 Earthquakes

If the impactor produces a crater, it must produce an earthquake. Work on buried nuclear explosives indicates that the Richter scale magnitude (see Fig. 18) produced by the release of a yield Y is given by

$$M=3.9+0.7\log_{10}(Y/kt) \quad (49)$$

(Barosh 1969). Here we identify Y as the energy impacting the ground. A relatively small fraction of the impact energy goes into the earthquake. Most of it goes into produc-

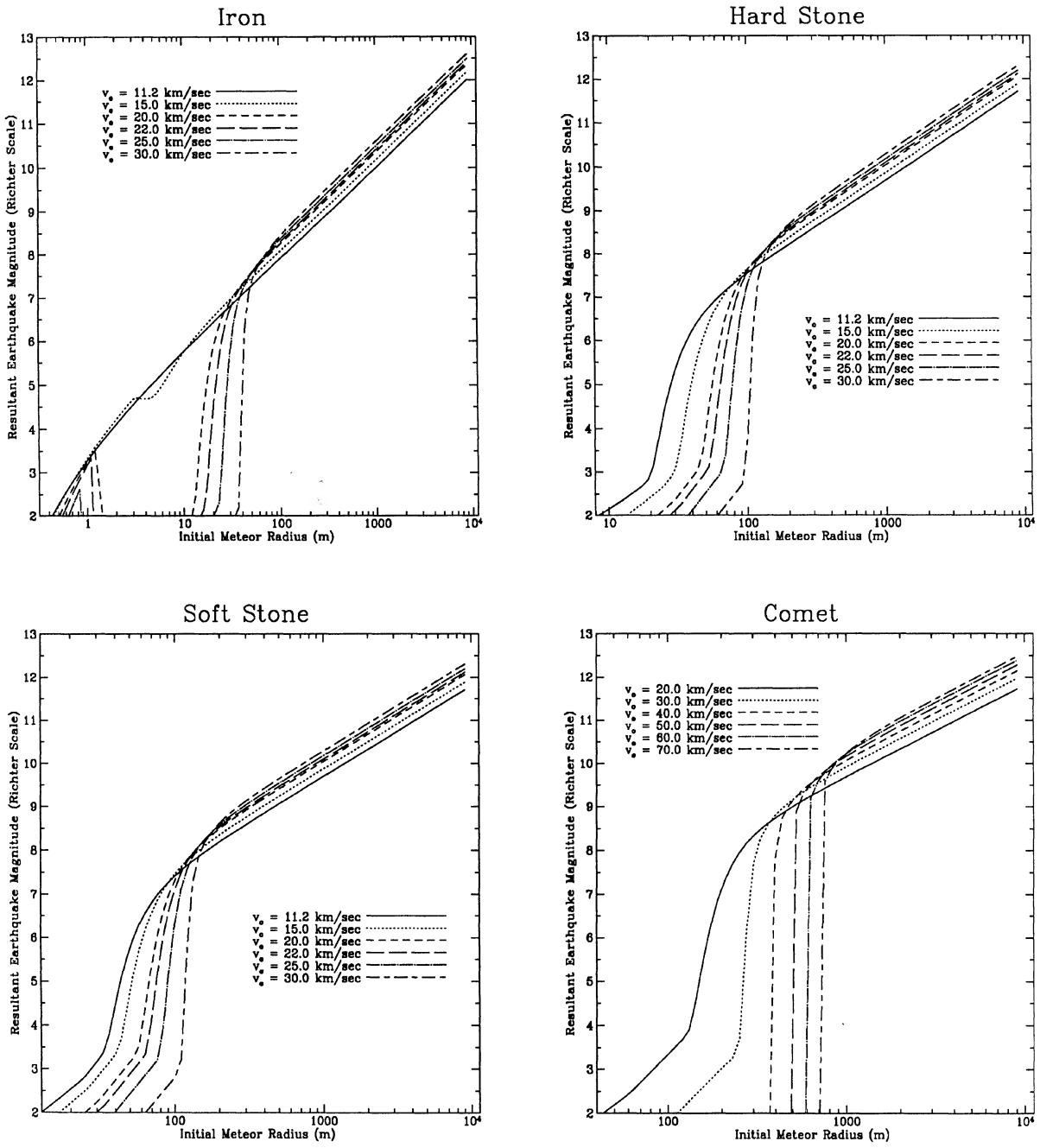

FIG. 18. The Richter scale magnitude of the earthquake produced by the impactor debris hitting the ground. This is given as a function of the initial radius of the impactor for various impact velocities and composition classes.

ing the crater in either a nuclear explosion or a meteorite impact. Figure 18 shows the earthquakes magnitudes produced by impactors as a function of impactor radius and velocity.

If the radius, R, of an asteroid is sufficiently large, the atmosphere is not effective in slowing it down, so it impacts the ground at nearly its original kinetic energy. This is true for stony meteorites with $R > 100$ m. For these objects, the earthquake magnitude is

$$M = 7.9 + 0.7\left[3\log_{10}\left(\frac{R}{100\ \text{m}}\right) + 2\log_{10}\left(\frac{V}{20\ \text{km/s}}\right) + \log_{10}\left(\frac{\rho_M}{3\ \text{g/cm}^3}\right)\right]. \quad (50)$$

A stony asteroid with a radius of 260 m and $V = 20$ km/s has an impact energy of $Y = 10$ gigatons and produces an earthquake of Richter scale 8.8, which equals that of the

largest earthquakes ever recorded. The Cretaceous–Tertiary impactor ($R \geqslant 5$ km) produced an earthquake with a minimum Richter magnitude of $M = 11.5$.

3.5.6 Deep water waves and tsunami

Waves caused by ocean impacts may be the most serious problem produced by impacting asteroids short of the massive killers such as the Cretaceous–Tertiary impactor. Just as on land, most of the kinetic energy of a large asteroid that impacts into the ocean goes into the formation of a crater, but the crater is not stable. The filling in of the crater and its subsequent rebound produces a series of waves that propagate radially away from the impact. Impacts into deep water produce surface waves that do not dampen significantly until they run into shallows where they steepen into breakers and increase in height to form tsunami (Mader 1988). The average tsunami is about 40 times higher than the deep water wave that produced it (Mader 1992). The height of a deep water wave only decreases with the inverse distance from the point of impact, so it can cause serious problems far from the impact point. This is a result of the wave being inherently two dimensional. The intensity of an inherently three-dimensional disturbance such as an airburst or an earthquake falls off as the inverse square of the distance, so such a disturbance is far more localized than water waves.

Experiments with underwater nuclear explosives show that the full height of a deep-water wave at a distance r from the underwater detonation of energy Y is given by

$$h_W = 40\ 500\ \text{ft}\frac{(Y/\text{kton})^{0.54}}{r/\text{ft}} = 22.7\ \text{m}\left(\frac{Y}{10\ \text{gigatons}}\right)^{0.54}\left(\frac{1000\ \text{km}}{r}\right) \quad (51)$$

(Glasstone & Dolan 1977). This result is not sensitive to the depth at which the explosion occurs. Figure 19 shows the height of deep water waves 1000 km from the impact point as a function of impactor radius for various impactor compositions and impact velocities. Here we have assumed that the impact energy is the value of Y used in Eq. (48).

For the larger asteroids, e.g., $R > 100$ m for stony asteroids, that suffer no significant energy dissipation in the atmosphere, the deep-water wave height at distance r is given by

$$h_W = 15.6\ \text{m}\left[\left(\frac{R}{203\ \text{m}}\right)^3\left(\frac{V}{20\ \text{km}}\right)^2\left(\frac{\rho_{\mathcal{M}}}{3\ \text{g/cm}^3}\right)\right]^{0.54} \times\left(\frac{1000\ \text{km}}{r}\right). \quad (52)$$

Here an asteroid with a radius of 203 m and a velocity of 20 km/s has an impact energy of 5 gigatons. An asteroid of this size or larger impacts the Earth about every 10^4 yr.

The wave duration (which is determined by the fill-in time of the water crater) increases with yield and is over 2 min for asteroids with $R > 150$ m. The deep-water wave velocity is several hundred kilometers/hour. As the deep-water wave goes into a shoal, its speed decreases and its front increases in sharpness and amplitude until it breaks. While the average increase in its height is about forty fold, locally it can be greater or less than this depending on the geometry of the bay. An asteroid with a radius of 200 m that drops anywhere in the mid Atlantic will produce deep water waves that are at least 5 m high when they reach both the European and North American coasts. When it encounters land, this wave steepens into a tsunami over 200 m in height that hits the coast with a pulse duration of at least 2 min, so it would move far inland before the pressure driving it stops. Low-lying areas such as Holland, Denmark, Long Island, or Manhattan may be washed out. (These numbers are very disturbing to the authors. Perhaps the legendary tale of the lost civilization of Atlantis, which was said to be on the Atlantic coast and was engulfed suddenly by the ocean was due to such a tidal wave. It is somewhat surprising that there were no widespread coastal settlements along the Atlantic until after 800 A.D. when the Vikings settled and fortified numerous towns along the Atlantic coast. The niche that they exploited may have been opened by a previous disaster whose institutional memory had been lost.)

Because a disproportionate fraction of human resources are close to the coasts, tsunami are probably the most deadly manifestations of asteroid impacts apart from the very large Cretaceous–Tertiary superkillers. Geological (and perhaps archaeological) evidence for large tsunamis along the coasts of the major oceans (due to their large cross sections) may be the best counters for moderately large ($R = 100$–1000 m) asteroid impacts.

4. CONCLUSIONS

We have investigated the effect of the atmosphere on impacting asteroids and comets. We have found that the atmosphere is ineffective in preventing impact damage to the ground when the radius of a stony asteroid exceeds 100 m and that of a comet exceeds 500 m. For iron meteorites that impact at greater than 20 km/s, the critical radius is about 20–30 m. For low-velocity iron meteorites that hit at 11.2–15 km/s, the critical radius is only 2 m. While the dissipation of energy in the atmosphere protects the ground from impact damage (craters, earthquakes, and tsunami), it can enhance the damage done by the airburst. The area of destruction produced by the airburst in the impact of small asteroids can be up to twice as large as it would have been had the same energy been released at sea level. Stony meteorites with radii greater than about 60 km put enough energy into the hot plume produced in their wake that the plume (or thermal) is not contained by the atmosphere. It breaks out of the atmosphere and floats around the Earth carrying any entraped dust with it. The deposition of this dust in the Antarctica and in Greenland icecaps may provide a counter for large meteorite impacts of the past few hundred thousand years.

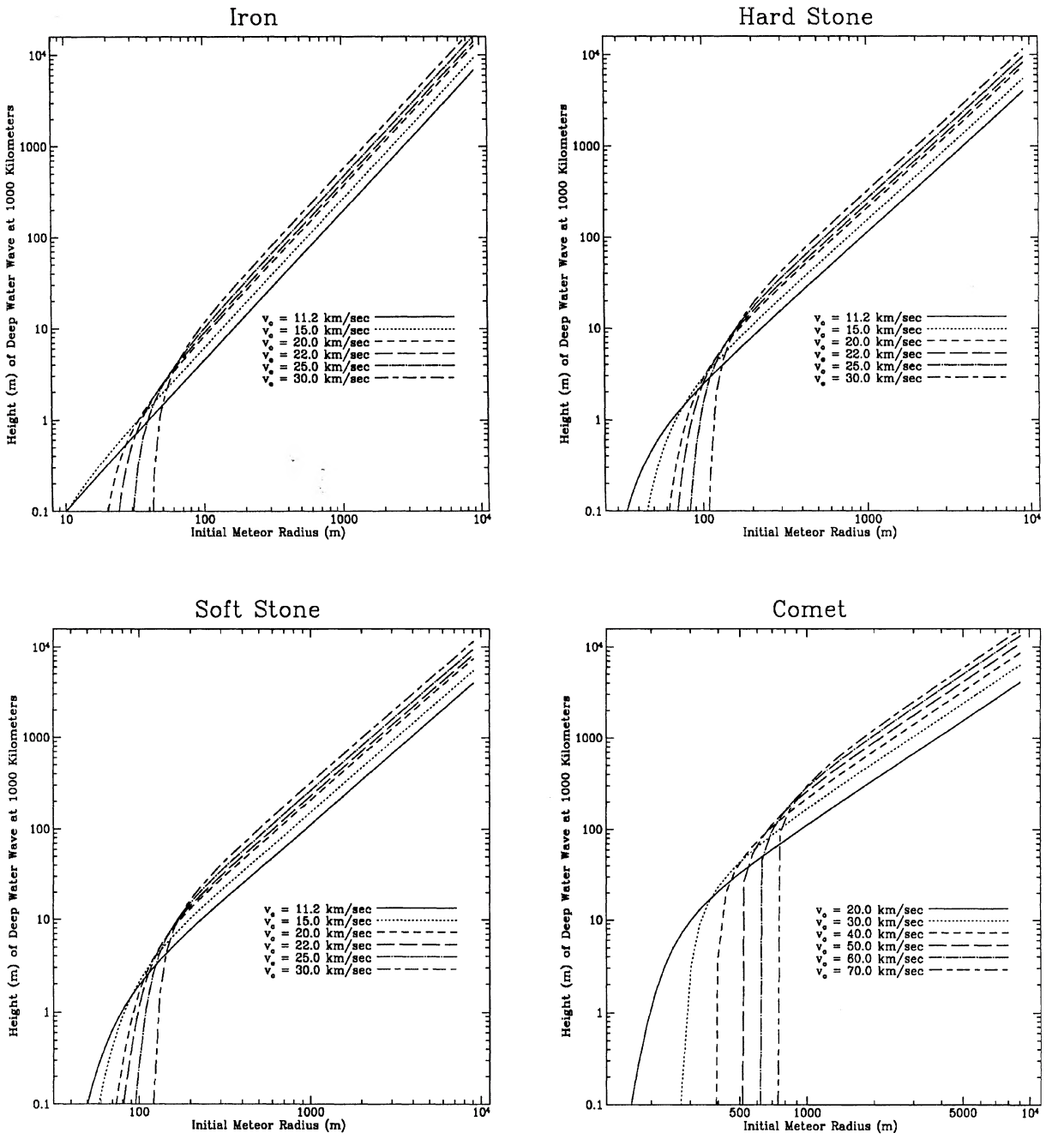

FIG. 19. The full height in meters of a deep-water wave 1000 km from the impact point in the ocean. This is given as a function of impactor radius for various impact velocities and composition types. The average height of the tsunami produced when these waves run into land is about 40 times that of the original deep-water wave.

We plan to study the effect of the atmospheres of Mars and Venus on impact collisions and crater distributions. We will also look at the effect of a curved atmosphere on impactors at large zenith angles. Hills *et al.* (1992) are estimating the economic damage done by asteroid impacts and the insurance premium that should be assigned to technologically preventing such disasters.

M.P.G. would like to thank the Department of Energy for an undergraduate SERS (Science and Engineering Research Semester) Fellowship that supported his work at Los Alamos. M.P.G. and J.G.H. would like to thank Johndale Solem for supplying Eq. (39) that determines the ground damage done by an airburst.

REFERENCES

Allen, C. W. 1973, Astrophysical Quantities (Athlone, London)

Alvarez, L., Alvarez, W., Asaro, F., & Michel, H. V. 1980, Science, 208, 1095

Bartky, C. D., Gordon, E., & Li, F. 1973, Sky and Tel. 45, 219

Barosh, P. J. 1969, Geological Survey Bulletin 1279

Bronshten, V. A. 1983, Physics of Meteoric Phenomena (Reidel, Dordrecht)

Brown, W. K. 1988, A Theory of Sequential Fragmentation and its Astronomical Applications, Los Alamos Technical Report LA-11043

Fessenkov, V. 1955, in Meteors, edited by T. R. Kaiser (Pergamon, New York)

Glasstone, S., & Dolan, P. J. 1977, The Effects of Nuclear Weapons, third Ed. (U.S. Government Printing Office, Washington, DC)

Halliday, I., Blackwell, A. T., & Griffin, A. A. 1985, Nature, 318, 317

Hills, J. G., Solem, J., & Goda, M. P. 1992, in preparation

Jones, E. M., & Kodis, J. W. 1982, Geological Society of America Special Paper 190

Mader, C. L. 1988, Numerical Modeling of Water Waves (University of California Press, Berkeley)

Mader, C. L. 1992, private communication

Morrison, David 1992, The Spaceguard Survey, Report of the NASA International Near-Earth-Object Detection Workshop, NASA Report

Nicholas, T., & Recht, R. F. 1990 in High Velocity Impact Dynamics, edited by J. A. Zukas (Wiley, New York)

Opik, E. J. 1958, Physics of Meteor Flight in the Atmosphere (Wiley, New York).

Petaev, M. I. 1992, Sky and Tel., 84, 127

Rather, J. D. G., Rahe, J. H., & Canavan, G. 1992, Summary Report of the Near-Earth-Object Interception Workshop, NASA Report.

Schultz, P. H., & Beatty, J. K. 1992, Sky and Tel., 83, 387

Schultz, P. H., & Lianza, R. E. 1992, Nature, 355, 234

Sekanina, Z. 1983, AJ, 88, 1382

Shoemaker, E. M., Wolfe, R. F., & Shoemaker, C. S. 1990, Geological Society of America Special Paper 247

Wolbach, W. S., Lewis, R. S., & Anders, E. 1985, Science, 230, 167